Available online at www.sciencedirect.com
SCIENCE DIRECT®
Journal of Molecular Spectroscopy 235 (2006) 35–53
Journal of MOLECULAR SPECTROSCOPY
www.elsevier.com/locate/jms

Measurements and theoretical calculations of N_2-broadening and N_2-shift coefficients in the v_2 band of CH_3D

Adriana Predoi-Cross [a,*], Kyle Hambrook [a], Marco Brawley-Tremblay [a], Jean-Pierre Bouanich [b], Mary Ann H. Smith [c]

[a] Physics Department, University of Lethbridge, 4401 University Drive, Lethbridge, Alta., Canada T1K 3M4
[b] Laboratoire de Photophysique Moléculaire, CNRS UPR3361, Université de Paris-Sud, Bâtiment 350, F-91405 Orsay, France
[c] Atmospheric Sciences, NASA Langley Research Center, MS 401A, Hampton, VA 23681-2199, USA

Received 28 September 2005; in revised form 3 October 2005
Available online 15 November 2005

Abstract

In this paper, we report measured Lorentz N_2-broadening and N_2-induced pressure-shift coefficients of CH_3D in the v_2 fundamental band using a multispectrum fitting technique. These measurements were made by analyzing 11 laboratory absorption spectra recorded at 0.0056 cm^{-1} resolution using the McMath-Pierce Fourier transform spectrometer located at the National Solar Observatory on Kitt Peak, Arizona. The spectra were obtained using two absorption cells with path lengths of 10.2 and 25 cm. The total sample pressures ranged from 0.98 to 402.25 Torr with CH_3D volume mixing ratios of 0.01 in nitrogen. We have been able to determine the N_2 pressure-broadening coefficients of 368 v_2 transitions with quantum numbers as high as $J'' = 20$ and $K = 16$, where $K'' = K' \equiv K$ (for a parallel band). The measured N_2-broadening coefficients range from 0.0248 to 0.0742 cm^{-1} atm^{-1} at 296 K. All the measured pressure-shifts are negative. The reported N_2-induced pressure-shift coefficients vary from about -0.0003 to -0.0094 cm^{-1} atm^{-1}. We have examined the dependence of the measured broadening and shift parameters on the J'', and K quantum numbers and also developed empirical expressions to describe the broadening coefficients in terms of m ($m = -J''$, J'', and $J'' + 1$ in the ^QP-, ^QQ-, and ^QR-branch, respectively) and K. On average, the empirical expressions reproduce the measured broadening coefficients to within 4.7%. The N_2-broadening and pressure-shift coefficients were calculated on the basis of a semiclassical model of interacting linear molecules performed by considering in addition to the electrostatic contributions the atom–atom Lennard-Jones potential. The theoretical results of the broadening coefficients are in good overall agreement with the experimental data (8.7%). The N_2-pressure shifts whose vibrational contribution is derived from parameters fitted in the ^QQ-branch of self-induced shifts of CH_3D, are also in reasonable agreement with the scattered experimental data (20% in most cases).

Keywords: Monodeuterated methane; CH_3D; N_2-broadening; Fourier transform infrared spectroscopy; Spectral lineshape

1. Introduction

Laboratory spectroscopic studies of the v_2 vibrational band of CH_3D are needed for the correct interpretation of atmospheric spectra of Jupiter, Saturn, and Titan, which have been and will be gathered by the Galileo and Cassini spacecrafts. The planetary atmospheres of Neptune and Uranus are also known to contain CH_3D. Of particular interest is the accurate determination of the CH_3D abundance and the D/H ratio in methane (via the CH_3D/CH_4 ratio) in the atmospheres of these solar system bodies. Significant differences in the thermodynamics and kinetics of various processes (e.g., chemical reactions, condensation, and thermal escape) result from the significant mass difference between H and its isotope D leading to an isotopic fractionation. For this reason, the D/H ratio in methane can provide invaluable insight into the formation and dynamics of the atmospheres of a number of solar system objects [1–4]. This work also has relevance to the $3v_2$ band

* Corresponding author. Fax: +1 403 329 2057.
E-mail address: Adriana.predoicross@uleth.ca (A. Predoi-Cross).

0022-2852/$ - see front matter © 2005 Elsevier Inc. All rights reserved.
doi:10.1016/j.jms.2005.10.003

of CH_3D and its importance in measuring the D/H ratio in the atmospheric methane of the giant planets and Titan [4,5], as broadening parameters do not vary substantially from one vibrational band to another of the same molecule.

This paper is a continuation of our study of spectroscopic line parameters in the ν_2 band of CH_3D [6]. The ν_2 band of $^{12}CH_3D$ is the lowest band ($\nu_0 \approx 2200\ cm^{-1}$) of a polyad of nine interacting vibrational states. Several studies of lineshape parameters for CH_3D perturbed by nitrogen have been reported. Recently, studies of N_2- and self-broadening and shifting in the ν_3, ν_5, and ν_6 bands of CH_3D have been published [7–9]. Varanasi and Chudamani [10] measured N_2-, self-, H_2-, and He-broadening coefficients for 4 transitions in the ν_6 band at temperatures of 123, 188, and 295 K. N_2-, H_2-, and self-broadening parameters for 10 ν_6 band transitions were reported by Lacome et al. [11]. Devi et al. [12] measured N_2- and air-broadening coefficients for 24 lines and self-broadening coefficients for 2 lines in the ν_6 band at room temperature. N_2-, air-, and self-broadening coefficients for several transitions in the ν_3 band were measured by Devi et al. [13]. Nitrogen-broadening parameters for 33 lines in the ν_3 band were measured by Blanquet et al. [14] using both Voigt and Rautian profiles. Walrand et al. [15] reported N_2- and O_2-broadening coefficients also measured by fitting the spectral profiles of transitions in the ν_3 band to both Voigt and Rautian models. Boussin et al. [4] published measurements of N_2-, H_2-, and He-broadening and pressure-shift coefficients in addition to empirical expressions for the broadening coefficients in the $3\nu_2$ overtone band. N_2-broadening in the ν_2 band of CH_3D has been the focus of very few studies. Varanasi et al. [16] derived an empirical expression for N_2-broadening coefficients along with a theoretically deduced self-broadening coefficient expression in this band. N_2- and H_2-broadening coefficients for 5 ^QP-branch transitions in the ν_2 band of CH_3D over a temperature range of 94–300 K were measured by Chudamani and Varanasi [17].

Several theoretical studies have been devoted to monodeuterated methane. Tejwani and Fox [18] calculated self-, N_2-, O_2-, and H_2-broadening coefficients at room and low temperatures from the Anderson–Tsao–Curnutte theory [19]. They have determined an effective value of 5.6 D $Å^2$ for the octopole moment of CH_3D. More recently, N_2-broadening coefficients of CH_3D were measured for 33 lines in the ν_3 band [14]. Using the semiclassical formulation of Robert and Bonamy [20] and the electrostatic potential considered in [18], much lower results (40–60%) than those reported by Tejwani and Fox were obtained [14]. It was indeed shown that the single electrostatic potential appears to be quite insufficient to explain the experimental measurements. Then, in addition to electrostatic interactions, we have considered the contributions obtained by Leavitt [21] for the induction and dispersion interactions [14]. However, our calculation has not provided satisfactory results for different reasons: (i) accurate potential parameters are not available for CH_3D, especially the polarizability anisotropy and higher polarizabilities; (ii) the dispersion contributions which are poorly known are predominant for this system; (iii) the anisotropic potential used does not take into account the repulsive interactions. Here, we consider a different theoretical approach recently applied to CH_3D–H_2 [22] as well as to self-broadening and self-induced shifts of CH_3D [6], approximating CH_3D as a linear molecule for its interactions with N_2 and involving the atom–atom Lennard-Jones potential, in addition to the electrostatic potential.

2. Experimental details

The absorption spectra used in this work were obtained using the McMath-Pierce Fourier transform spectrometer (FTS) of the National Solar Observatory (NSO) on Kitt Peak. The spectra were recorded at an unapodized resolution of $0.0056\ cm^{-1}$ spectral range using two absorption cells with path lengths of 10.2 and 25 cm. The spectra were used previously for a similar study of the ν_3 band [7].

Eleven spectra covering the 2048–2318 cm^{-1} were simultaneously fit using a multispectrum nonlinear least-squares procedure [23]. Using this novel analysis tool, we were able to combine spectra recorded with low pressures of 98% pure CH_3D, self-broadened spectra, and lean mixtures ($\sim$1%) of CH_3D in N_2 in a single least-squares solution. A summary of the experimental conditions for each spectrum is given in Table 1. The experimental setup and data reduction methods were described in detail in our earlier study [6]. The wavenumber calibration for the CH_3D line positions was performed with respect to the well-known line centers of water [24].

An example of a multispectrum fitted interval is presented in Fig. 1. The top panel shows P-branch transitions with $J'' = 16$ and K values from 0 to 12. All 11 spectra were included in the least-squares solution. The bottom panel indicates the fit residuals (observed minus calculated for all 11 spectra). A small quantity of carbon monoxide was present in the sample producing "extra" lines in our spectra. One such transition is shown in Fig. 1. The positions of transitions due to contaminants were determined prior to

Table 1
Summary of experimental conditions of CH_3D spectra

Temperature (K)	Broadener gas	CH_3D volume mixing ratio	Path (cm)	Pressure (Torr)
300.2	$^{12}CH_3D$	1	10.2	0.98
300.0	$^{12}CH_3D$	1	10.2	2.95
300.7	$^{12}CH_3D$	1	10.2	17.50
300.7	$^{12}CH_3D$	1	10.2	79.00
300.2	$^{12}CH_3D$	1	10.2	110.00
299.8	$^{12}CH_3D$	1	10.2	152.00
299.8	$^{12}CH_3D$	1	10.2	303.00
299.2	N_2	0.01	25	102.50
299.4	N_2	0.01	25	202.10
299.5	N_2	0.01	25	302.55
299.4	N_2	0.01	25	402.25

Note. 760 Torr = 1 atm = 101.325 kPa.

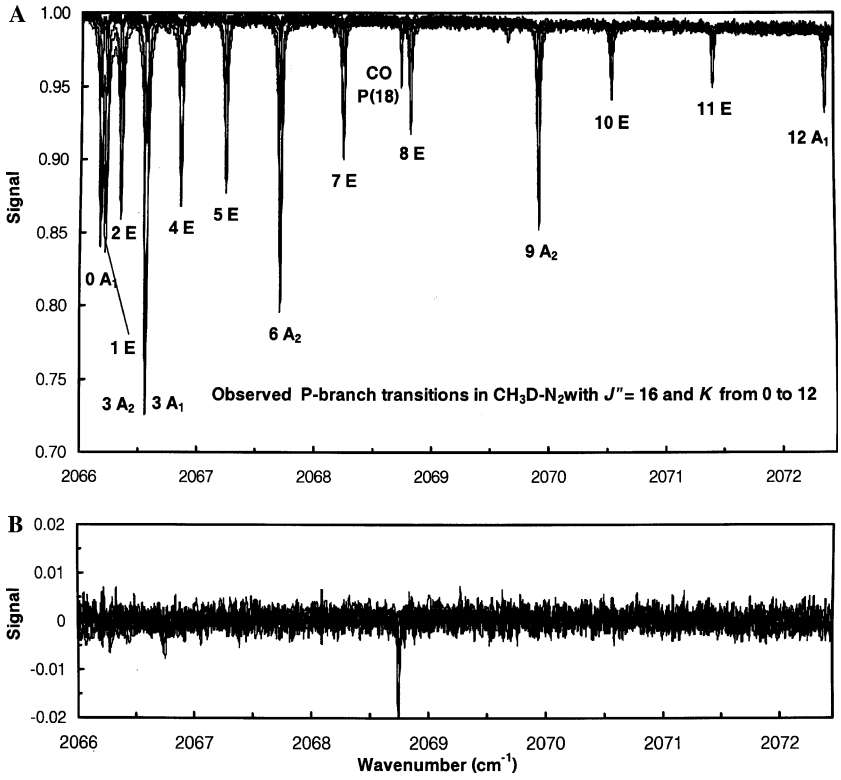

Fig. 1. An example of a multispectrum fitted interval in the ν_2 band of $^{12}CH_3D$ near 2069 cm^{-1}. A spectral region of 6.5 cm^{-1} was fitted simultaneously in each of the 11 spectra. All experimental spectra are overlaid in the top panel (A). Noticeable in (A) is a CO transition present in the spectrum as a contaminant and used for wavenumber calibration. (B) The (observed − calculated) fit residuals are plotted.

using the multispectrum fitting procedure. These lines were fit in the least-squares solution using 0.075 cm^{-1} atm^{-1} at 296 K as N_2-broadening and −0.006 cm^{-1} atm^{-1} as N_2-induced pressure-shift coefficients, respectively.

3. Results and discussion

The N_2-broadening coefficients and N_2-pressure induced shift coefficients for CH_3D transitions in the ν_2 band retrieved from our multispectrum analysis are presented in Table 2. They are given in units of cm^{-1} atm^{-1} at 296 K. For each transition, we list the line center positions retrieved from the fits (in cm^{-1}) and the transitions quantum numbers. In our analysis, we have not applied any temperature corrections to the measured pressure-shift coefficients. Hence, the pressure-shift coefficients listed in Table 2 correspond to values at the mean temperature (298 ± 2 K) at which the spectra were recorded. We present our results arranged in groups of ^{Q}P-, ^{Q}Q-, and ^{Q}R-branches. Within each branch, the results are arranged separately for the A- and E-species transitions. The values in parentheses in Table 2 represent one standard deviation uncertainties in the measured quantities in units of the last quoted digit.

3.1. Discussion of the measured N_2-broadening coefficients

In Fig. 2, we have plotted all measured $\gamma(N_2)$ values for the ν_2 transitions as a function of m ($m = -J''$, J'', $J''+1$ for ^{Q}P-, ^{Q}Q-, and ^{Q}R-branch lines, respectively). We have plotted the N_2-broadening coefficients for the ^{Q}Q-branch $J'' = K$ transitions with a different symbol to highlight their unusual pattern and smaller size.

In Fig. 3, we have plotted the ratio of our measured N_2-broadening coefficients to broadening coefficients from previous studies. In Fig. 3A, the ratio is with respect to the N_2-broadening coefficients reported by Devi et al. [7] for the ν_3 band. The mean ratio of N_2-broadening coefficients is 0.99(3) highlighting the very good agreement between our N_2-broadening coefficients and transitions with the same quantum numbers and symmetry species of the ν_3 band [7]. In Fig. 3B, we have plotted the ratio of our measured N_2-broadening coefficients to broadening coefficients from the study of the $3\nu_2$ band of Boussin et al. [5]. The mean ratio is in this case 1.02(6).

Additional comparisons with previous spectroscopic studies are presented in Table 3, indicating a good agreement with all sets of measurements. We have also calculated the average ratio of our N_2-broadening coefficients for ^{Q}P-branch to ^{Q}R-branch lines of the same $|m|$ and K to be 1.04(5). For transitions with $K \leqslant 2$ and $K \leqslant 1$ this ratio is 1.02(4) and 1.02(5), respectively. Based on these statistics, we estimate that the absolute uncertainty of our reported broadening coefficients is no worse than 3%.

We have fitted the experimental N_2-broadening coefficients to empirical expressions as previously done in [6,7]. The broadening coefficients for all transitions except

Table 2
Measured and calculated zero-pressure line positions, N_2-broadening coefficients, and N_2-induced pressure-shift coefficients in the v_2 band of CH_3D

Position[a,b]	J'	K'	N'	J''	K''	N''	Assignment	Measured $\gamma(N_2)$[a,c]	Measured $\delta(N_2)$[a,d]	Calculated $\gamma(N_2)$[c]	Calculated $\delta(N_2)$[c]
2048.477200(99)	17	3	*A*2	18	3	*A*1	*QP*(18,3,*A*1)	0.0497(4)		0.0444	−0.00589
2051.910190(83)	17	9	*A*2	18	9	*A*1	*QP*(18,9,*A*1)	0.0425(6)		0.0495	−0.00568
2057.622324(75)	16	3	*A*2	17	3	*A*1	*QP*(17,3,*A*1)	0.0581(2)		0.0466	−0.00580
2063.506279(96)	16	12	*A*2	17	12	*A*1	*QP*(17,12,*A*1)	0.0416(4)		0.0504	−0.00583
2066.273108(96)	15	0	*A*2	16	0	*A*1	*QP*(16,0,*A*1)	0.0556(6)		0.0476	−0.00574
2066.657119(99)	15	3	*A*2	16	3	*A*1	*QP*(16,3,*A*1)	0.0563(5)		0.0488	−0.00572
2070.022716(27)	15	9	*A*2	16	9	*A*1	*QP*(16,9,*A*1)	0.0514(2)		0.0529	−0.00556
2072.476313(99)	15	12	*A*2	16	12	*A*1	*QP*(16,12,*A*1)	0.0406(5)		0.0513	−0.00589
2075.615203(17)	14	3	*A*2	15	3	*A*1	*QP*(15,3,*A*1)	0.0558(3)		0.0509	−0.00563
2076.758062(31)	14	6	*A*2	15	6	*A*1	*QP*(15,6,*A*1)	0.0525(2)	−0.00739(18)	0.0534	−0.00552
2078.961714(49)	14	9	*A*2	15	9	*A*1	*QP*(15,9,*A*1)	0.0516(4)	−0.00561(25)	0.0544	−0.00553
2084.107231(46)	13	0	*A*2	14	0	*A*1	*QP*(14,0,*A*1)	0.0602(10)	−0.00265(12)	0.0519	−0.00556
2084.488044(27)	13	3	*A*2	14	3	*A*1	*QP*(14,3,*A*1)	0.0563(3)	−0.00447(18)	0.0531	−0.00554
2087.831217(45)	13	9	*A*2	14	9	*A*1	*QP*(14,9,*A*1)	0.0493(3)	−0.00308(18)	0.0557	−0.00553
2094.404300(22)	12	6	*A*2	13	6	*A*1	*QP*(13,6,*A*1)	0.0530(2)	−0.00428(10)	0.0572	−0.00535
2096.654056(35)	12	9	*A*2	13	9	*A*1	*QP*(13,9,*A*1)	0.0516(5)	−0.00301(14)	0.0568	−0.00558
2101.989013(17)	11	3	*A*2	12	3	*A*1	*QP*(12,3,*A*1)	0.0562(9)	−0.00409(31)	0.0572	−0.00534
2103.105182(18)	11	6	*A*2	12	6	*A*1	*QP*(12,6,*A*1)	0.0544(4)	−0.00475(29)	0.0590	−0.00529
2105.492395(59)	11	9	*A*2	12	9	*A*1	*QP*(12,9,*A*1)	0.0543(3)	−0.00605(13)	0.0576	−0.00571
2111.726736(13)	10	6	*A*2	11	6	*A*1	*QP*(11,6,*A*1)	0.0561(4)	−0.00493(35)	0.0606	−0.00525
2113.320521(48)	10	9	*A*2	11	9	*A*1	*QP*(11,9,*A*1)	0.0587(2)	−0.00957(18)	0.0579	−0.00597
2118.805528(56)	9	0	*A*2	10	0	*A*1	*QP*(10,0,*A*1)	0.0625(3)	−0.00490(32)	0.0602	−0.00518
2119.173157(45)	9	3	*A*2	10	3	*A*1	*QP*(10,3,*A*1)	0.0566(3)	−0.00390(23)	0.0612	−0.00516
2120.269672(15)	9	6	*A*2	10	6	*A*1	*QP*(10,6,*A*1)	0.0619(3)	−0.00536(29)	0.0620	−0.00526
2135.684279(15)	7	0	*A*2	8	0	*A*1	*QP*(8,0,*A*1)	0.0634(3)	−0.00407(28)	0.0641	−0.00501
2136.045289(18)	7	3	*A*2	8	3	*A*1	*QP*(8,3,*A*1)	0.0605(7)	−0.00428(14)	0.0650	−0.00501
2152.251071(23)	5	0	*A*2	6	0	*A*1	*QP*(6,0,*A*1)	0.0640(3)	−0.00481(28)	0.0677	−0.00486
2152.605761(10)	5	3	*A*2	6	3	*A*1	*QP*(6,3,*A*1)	0.0624(5)	−0.00546(24)	0.0679	−0.00488
2168.503102(12)	3	0	*A*2	4	0	*A*1	*QP*(4,0,*A*1)	0.0672(3)	−0.00469(30)	0.0704	−0.00456
2184.434726(28)	1	0	*A*2	2	0	*A*1	*QP*(2,0,*A*1)	0.0680(7)	−0.00234(10)	0.0719	−0.00458
2048.492027(94)	17	3	*A*1	18	3	*A*2	*QP*(18,3,*A*2)	0.0497(4)		0.0444	−0.00589
2049.642192(28)	17	6	*A*1	18	6	*A*2	*QP*(18,6,*A*2)	0.0442(7)		0.0472	−0.00577
2051.878222(67)	17	9	*A*1	18	9	*A*2	*QP*(18,9,*A*2)	0.0425(6)		0.0495	−0.00568
2054.440995(43)	17	12	*A*1	18	12	*A*2	*QP*(18,12,*A*2)	0.0420(9)		0.0493	−0.00580
2057.228713(78)	16	0	*A*1	17	0	*A*2	*QP*(17,0,*A*2)	0.0494(8)		0.0455	−0.00582
2057.611910(30)	16	3	*A*1	17	3	*A*2	*QP*(17,3,*A*2)	0.0581(2)		0.0466	−0.00580
2058.771403(81)	16	6	*A*1	17	6	*A*2	*QP*(17,6,*A*2)	0.0462(9)		0.0493	−0.00569
2067.808812(19)	15	6	*A*1	16	6	*A*2	*QP*(16,6,*A*2)	0.0520(8)	−0.00849(21)	0.0513	−0.00560
2075.232300(65)	14	0	*A*1	15	0	*A*2	*QP*(15,0,*A*2)	0.0578(7)	−0.00278(20)	0.0498	−0.00565
2085.622587(28)	13	6	*A*1	14	6	*A*2	*QP*(14,6,*A*2)	0.0555(8)	−0.00611(49)	0.0553	−0.00543
2092.900939(36)	12	0	*A*1	13	0	*A*2	*QP*(13,0,*A*2)	0.0622(8)	−0.00430(9)	0.0541	−0.00547
2093.278607(22)	12	3	*A*1	13	3	*A*2	*QP*(13,3,*A*2)	0.0565(3)	−0.00376(31)	0.0552	−0.00544
2110.249343(31)	10	0	*A*1	11	0	*A*2	*QP*(11,0,*A*2)	0.0626(8)	−0.00349(3)	0.0582	−0.00527
2110.620185(22)	10	3	*A*1	11	3	*A*2	*QP*(11,3,*A*2)	0.0560(8)	−0.00424(18)	0.0592	−0.00525
2122.013448(42)	9	9	*A*1	10	9	*A*2	*QP*(10,9,*A*2)	0.0625(7)	−0.00868(10)	0.0574	−0.00632
2127.283841(32)	8	0	*A*1	9	0	*A*2	*QP*(9,0,*A*2)	0.0624(12)	−0.00429(16)	0.0622	−0.00509
2127.648137(25)	8	3	*A*1	9	3	*A*2	*QP*(9,3,*A*2)	0.0556(8)	−0.00623(17)	0.0632	−0.00508
2128.734690(18)	8	6	*A*1	9	6	*A*2	*QP*(9,6,*A*2)	0.0601(8)	−0.00642(12)	0.0629	−0.00532
2137.122108(16)	7	6	*A*1	8	6	*A*2	*QP*(8,6,*A*2)	0.0650(7)	−0.00604(15)	0.0630	−0.00549
2144.006844(18)	6	0	*A*1	7	0	*A*2	*QP*(7,0,*A*2)	0.0652(4)	−0.00401(8)	0.0660	−0.00494
2144.364711(11)	6	3	*A*1	7	3	*A*2	*QP*(7,3,*A*2)	0.0597(5)	−0.00449(14)	0.0667	−0.00495
2145.431915(64)	6	6	*A*1	7	6	*A*2	*QP*(7,6,*A*2)	0.0714(3)	−0.00545(24)	0.0615	−0.00591
2160.416790(14)	4	0	*A*1	5	0	*A*2	*QP*(5,0,*A*2)	0.0656(7)	−0.00473(27)	0.0692	−0.00473
2160.768618(13)	4	3	*A*1	5	3	*A*2	*QP*(5,3,*A*2)	0.0657(4)	−0.00641(19)	0.0686	−0.00495
2168.852083(12)	3	3	*A*1	4	3	*A*2	*QP*(4,3,*A*2)	0.0703(9)	−0.00634(27)	0.0668	−0.00528
2176.509393(13)	2	0	*A*1	3	0	*A*2	*QP*(3,0,*A*2)	0.0672(9)	−0.00588(21)	0.0713	−0.00449
2192.277953(79)	0	0	*A*1	1	0	*A*2	*QP*(1,0,*A*2)	0.0675(4)		0.0729	−0.00484
2048.137645(49)	17	1	*E*	18	1	*E*	*QP*(18,1,*E*)	0.0444(9)		0.0434	−0.00591
2052.571852(68)	17	10	*E*	18	10	*E*	*QP*(18,10,*E*)	0.0422(8)		0.0498	−0.00568

[a] The values in parentheses represent one standard deviation uncertainties in the measured quantities in units of the last quoted digit.
[b] cm^{-1}.
[c] cm^{-1} atm^{-1} at 296 K.
[d] cm^{-1} atm^{-1} at the temperature of the spectra.

Table 2 (*continued*)

Position[a,b]	J'	K'	N'	J''	K''	N''	Assignment	Measured $\gamma(N_2)$[a,c]	Measured $\delta(N_2)$[a,d]	Calculated $\gamma(N_2)$[c]	Calculated $\delta(N_2)$[c]
2057.271463(88)	16	1	*E*	17	1	*E*	*QP*(17,1,*E*)	0.0520(9)		0.0456	−0.00583
2057.401225(76)	16	2	*E*	17	2	*E*	*QP*(17,2,*E*)	0.0530(8)		0.0460	−0.00583
2057.917807(78)	16	4	*E*	17	4	*E*	*QP*(17,4,*E*)	0.0498(3)		0.0474	−0.00577
2058.303626(46)	16	5	*E*	17	5	*E*	*QP*(17,5,*E*)	0.0444(10)		0.0483	−0.00573
2062.531933(31)	16	11	*E*	17	11	*E*	*QP*(17,11,*E*)	0.0440(3)		0.0511	−0.00571
2066.316582(14)	15	1	*E*	16	1	*E*	*QP*(16,1,*E*)	0.0518(2)		0.0478	−0.00575
2066.958728(27)	15	4	*E*	16	4	*E*	*QP*(16,4,*E*)	0.0589(9)		0.0496	−0.00569
2067.343002(32)	15	5	*E*	16	5	*E*	*QP*(16,5,*E*)	0.0555(9)		0.0505	−0.00564
2068.926869(46)	15	8	*E*	16	8	*E*	*QP*(16,8,*E*)	0.0471(2)		0.0527	−0.00555
2070.646321(68)	15	10	*E*	16	10	*E*	*QP*(16,10,*E*)	0.0438(8)		0.0528	−0.00562
2071.513983(75)	15	11	*E*	16	11	*E*	*QP*(16,11,*E*)	0.0429(10)		0.0522	−0.00573
2075.402152(28)	14	2	*E*	15	2	*E*	*QP*(15,2,*E*)	0.0584(10)	−0.00316(4)	0.0503	−0.00565
2075.912859(30)	14	4	*E*	15	4	*E*	*QP*(15,4,*E*)	0.0546(10)	−0.00223(13)	0.0517	−0.00559
2076.294413(50)	14	5	*E*	15	5	*E*	*QP*(15,5,*E*)	0.0525(10)	−0.00571(17)	0.0526	−0.00555
2077.299115(65)	14	7	*E*	15	7	*E*	*QP*(15,7,*E*)	0.0492(9)		0.0540	−0.00549
2077.890510(80)	14	8	*E*	15	8	*E*	*QP*(15,8,*E*)	0.0476(8)		0.0544	−0.00549
2079.548958(34)	14	10	*E*	15	10	*E*	*QP*(15,10,*E*)	0.0458(16)		0.0540	−0.00563
2084.149540(46)	13	1	*E*	14	1	*E*	*QP*(14,1,*E*)	0.0609(9)	−0.00271(17)	0.0521	−0.00557
2084.276619(47)	13	2	*E*	14	2	*E*	*QP*(14,2,*E*)	0.0601(16)	−0.00448(10)	0.0525	−0.00556
2084.783318(51)	13	4	*E*	14	4	*E*	*QP*(14,4,*E*)	0.0558(16)	−0.00641(21)	0.0538	−0.00550
2085.161942(44)	13	5	*E*	14	5	*E*	*QP*(14,5,*E*)	0.0565(1)	−0.00398(24)	0.0546	−0.00546
2086.161526(53)	13	7	*E*	14	7	*E*	*QP*(14,7,*E*)	0.0503(9)	−0.00308(26)	0.0558	−0.00542
2086.761133(68)	13	8	*E*	14	8	*E*	*QP*(14,8,*E*)	0.0505(8)		0.0560	−0.00545
2088.367064(22)	13	10	*E*	14	10	*E*	*QP*(14,10,*E*)	0.0503(1)		0.0550	−0.00569
2089.216173(78)	13	11	*E*	14	11	*E*	*QP*(14,11,*E*)	0.0503(9)		0.0540	−0.00595
2092.942913(35)	12	1	*E*	13	1	*E*	*QP*(13,1,*E*)	0.0585(15)	−0.00297(12)	0.0542	−0.00548
2093.068981(36)	12	2	*E*	13	2	*E*	*QP*(13,2,*E*)	0.0610(8)	−0.00430(31)	0.0546	−0.00546
2093.571575(40)	12	4	*E*	13	4	*E*	*QP*(13,4,*E*)	0.0552(8)	−0.00431(8)	0.0559	−0.00540
2093.947131(32)	12	5	*E*	13	5	*E*	*QP*(13,5,*E*)	0.0580(3)	−0.00470(77)	0.0566	−0.00537
2094.940263(36)	12	7	*E*	13	7	*E*	*QP*(13,7,*E*)	0.0526(16)		0.0575	−0.00537
2095.543263(47)	12	8	*E*	13	8	*E*	*QP*(13,8,*E*)	0.0499(17)		0.0574	−0.00544
2097.102388(91)	12	10	*E*	13	10	*E*	*QP*(13,10,*E*)	0.0539(3)		0.0558	−0.00583
2097.943146(78)	12	11	*E*	13	11	*E*	*QP*(13,11,*E*)	0.0537(16)		0.0547	−0.00622
2101.656303(26)	11	1	*E*	12	1	*E*	*QP*(12,1,*E*)	0.0617(17)	−0.00383(9)	0.0563	−0.00538
2101.781182(26)	11	2	*E*	12	2	*E*	*QP*(12,2,*E*)	0.0606(16)	−0.00600(83)	0.0566	−0.00537
2102.279459(29)	11	4	*E*	12	4	*E*	*QP*(12,4,*E*)	0.0586(12)	−0.00582(11)	0.0579	−0.00531
2102.651833(26)	11	5	*E*	12	5	*E*	*QP*(12,5,*E*)	0.0537(8)	−0.00471(12)	0.0585	−0.00529
2103.637422(31)	11	7	*E*	12	7	*E*	*QP*(12,7,*E*)	0.0514(8)		0.0591	−0.00534
2104.240866(42)	11	8	*E*	12	8	*E*	*QP*(12,8,*E*)	0.0525(13)	−0.00567(9)	0.0586	−0.00548
2105.758590(22)	11	10	*E*	12	10	*E*	*QP*(12,10,*E*)	0.0546(7)		0.0563	−0.00610
2106.589439(11)	11	11	*E*	12	11	*E*	*QP*(12,11,*E*)	0.0578(20)		0.0549	−0.00653
2110.290514(21)	10	1	*E*	11	1	*E*	*QP*(11,1,*E*)	0.0616(8)	−0.00270(14)	0.0583	−0.00528
2110.414345(26)	10	2	*E*	11	2	*E*	*QP*(11,2,*E*)	0.0603(8)	−0.00495(20)	0.0587	−0.00527
2110.908116(23)	10	4	*E*	11	4	*E*	*QP*(11,4,*E*)	0.0580(8)	−0.00423(21)	0.0599	−0.00522
2111.277157(70)	10	5	*E*	11	5	*E*	*QP*(11,5,*E*)	0.0563(8)	−0.00471(11)	0.0604	−0.00522
2112.254819(26)	10	7	*E*	11	7	*E*	*QP*(11,7,*E*)	0.0569(7)	−0.00608(25)	0.0603	−0.00537
2112.857014(38)	10	8	*E*	11	8	*E*	*QP*(11,8,*E*)	0.0544(10)	−0.00675(17)	0.0594	−0.00559
2114.336050(97)	10	10	*E*	11	10	*E*	*QP*(11,10,*E*)	0.0597(9)		0.0561	−0.00643
2118.846432(56)	9	1	*E*	10	1	*E*	*QP*(10,1,*E*)	0.0630(16)	−0.00365(6)	0.0603	−0.00518
2118.969092(57)	9	2	*E*	10	2	*E*	*QP*(10,2,*E*)	0.0600(8)	−0.00553(24)	0.0607	−0.00517
2119.458349(62)	9	4	*E*	10	4	*E*	*QP*(10,4,*E*)	0.0568(8)	−0.00381(20)	0.0618	−0.00515
2119.824145(19)	9	5	*E*	10	5	*E*	*QP*(10,5,*E*)	0.0568(8)	−0.00419(26)	0.0621	−0.00517
2120.793583(32)	9	7	*E*	10	7	*E*	*QP*(10,7,*E*)	0.0579(8)	−0.00574(21)	0.0612	−0.00546
2121.393229(59)	9	8	*E*	10	8	*E*	*QP*(10,8,*E*)	0.0602(8)	−0.00774(22)	0.0595	−0.00582
2127.324276(32)	8	1	*E*	9	1	*E*	*QP*(9,1,*E*)	0.0649(7)	−0.00457(7)	0.0623	−0.00509
2127.445906(32)	8	2	*E*	9	2	*E*	*QP*(9,2,*E*)	0.0603(7)	−0.00573(35)	0.0627	−0.00509
2127.930853(17)	8	4	*E*	9	4	*E*	*QP*(9,4,*E*)	0.0593(7)	−0.00486(40)	0.0636	−0.00509
2128.293178(22)	8	5	*E*	9	5	*E*	*QP*(9,5,*E*)	0.0605(8)	−0.00572(46)	0.0636	−0.00515
2129.254181(47)	8	7	*E*	9	7	*E*	*QP*(9,7,*E*)	0.0628(7)	−0.00715(99)	0.0613	−0.00566
2129.850320(92)	8	8	*E*	9	8	*E*	*QP*(9,8,*E*)	0.0660(18)		0.0587	−0.00620
2135.724332(24)	7	1	*E*	8	1	*E*	*QP*(8,1,*E*)	0.0617(7)	−0.00383(4)	0.0642	−0.00501
2135.844879(17)	7	2	*E*	8	2	*E*	*QP*(8,2,*E*)	0.0611(7)	−0.00577(26)	0.0646	−0.00501
2136.325434(18)	7	4	*E*	8	4	*E*	*QP*(8,4,*E*)	0.0619(7)	−0.00416(33)	0.0652	−0.00505

(*continued on next page*)

Table 2 (*continued*)

Position[a,b]	J'	K'	N'	J''	K''	N''	Assignment	Measured $\gamma(N_2)$[a,c]	Measured $\delta(N_2)$[a,d]	Calculated $\gamma(N_2)$[c]	Calculated $\delta(N_2)$[c]
2136.684549(20)	7	5	*E*	8	5	*E*	*QP*(8,5,*E*)	0.0626(6)	−0.00530(24)	0.0647	−0.00518
2137.637119(88)	7	7	*E*	8	7	*E*	*QP*(8,7,*E*)	0.0689(7)	−0.00595(26)	0.0601	−0.00606
2144.046535(14)	6	1	*E*	7	1	*E*	*QP*(7,1,*E*)	0.0644(7)	−0.00497(7)	0.0661	−0.00494
2144.166017(14)	6	2	*E*	7	2	*E*	*QP*(7,2,*E*)	0.0627(7)	−0.00549(24)	0.0664	−0.00494
2144.642158(29)	6	4	*E*	7	4	*E*	*QP*(7,4,*E*)	0.0625(19)	−0.00476(20)	0.0664	−0.00503
2152.290549(15)	5	1	*E*	6	1	*E*	*QP*(6,1,*E*)	0.0626(8)	−0.00435(8)	0.0678	−0.00485
2152.408930(15)	5	2	*E*	6	2	*E*	*QP*(6,2,*E*)	0.0658(9)	−0.00505(24)	0.0680	−0.00484
2152.881132(19)	5	4	*E*	6	4	*E*	*QP*(6,4,*E*)	0.0702(5)	−0.00561(48)	0.0667	−0.00512
2153.233986(28)	5	5	*E*	6	5	*E*	*QP*(6,5,*E*)	0.0702(7)	−0.00600(48)	0.0631	−0.00574
2160.454886(15)	4	1	*E*	5	1	*E*	*QP*(5,1,*E*)	0.0637(7)	−0.00438(30)	0.0693	−0.00472
2161.041516(24)	4	4	*E*	5	4	*E*	*QP*(5,4,*E*)	0.0741(4)	−0.00734(20)	0.0648	−0.00553
2168.539791(26)	3	1	*E*	4	1	*E*	*QP*(4,1,*E*)	0.0655(7)	−0.00312(28)	0.0705	−0.00458
2168.658349(13)	3	2	*E*	4	2	*E*	*QP*(4,2,*E*)	0.0659(8)	−0.00610(27)	0.0703	−0.00478
2176.547952(13)	2	1	*E*	3	1	*E*	*QP*(3,1,*E*)	0.0665(8)	−0.00412(33)	0.0715	−0.00460
2176.663450(20)	2	2	*E*	3	2	*E*	*QP*(3,2,*E*)	0.0709(12)	−0.00457(23)	0.0691	−0.00504
2184.472902(32)	1	1	*E*	2	1	*E*	*QP*(2,1,*E*)	0.0700(7)	−0.00528(26)	0.0714	−0.00485
2181.539436(80)	20	3	*A*2	20	3	*A*1	*QQ*(20,3,*A*1)	0.0434(7)		0.0366	−0.00601
2187.963182(78)	17	6	*A*2	17	6	*A*1	*QQ*(17,6,*A*1)	0.0437(6)		0.0447	−0.00579
2189.527781(88)	16	6	*A*2	16	6	*A*1	*QQ*(16,6,*A*1)	0.0435(5)		0.0468	−0.00570
2193.022326(51)	15	9	*A*2	15	9	*A*1	*QQ*(15,9,*A*1)	0.0429(3)	−0.00699(28)	0.0499	−0.00558
2191.281338(51)	14	3	*A*2	14	3	*A*1	*QQ*(14,3,*A*1)	0.0593(3)		0.0501	−0.00556
2196.531692(63)	14	12	*A*2	14	12	*A*1	*QQ*(14,12,*A*1)	0.0481(4)		0.0520	−0.00541
2192.529256(33)	13	3	*A*2	13	3	*A*1	*QQ*(13,3,*A*1)	0.0607(3)	−0.00557(26)	0.0522	−0.00547
2195.626335(93)	13	9	*A*2	13	9	*A*1	*QQ*(13,9,*A*1)	0.0490(2)	−0.00550(21)	0.0540	−0.00538
2195.678825(93)	10	3	*A*2	10	3	*A*1	*QQ*(10,3,*A*1)	0.0628(8)		0.0584	−0.00515
2196.714028(39)	10	6	*A*2	10	6	*A*1	*QQ*(10,6,*A*1)	0.0555(3)		0.0586	−0.00514
2196.545009(92)	9	3	*A*2	9	3	*A*1	*QQ*(9,3,*A*1)	0.0646(5)		0.0603	−0.00503
2197.318489(69)	8	3	*A*2	8	3	*A*1	*QQ*(8,3,*A*1)	0.0634(6)		0.0622	−0.00490
2198.002310(79)	7	3	*A*2	7	3	*A*1	*QQ*(7,3,*A*1)	0.0580(5)		0.0639	−0.00478
2199.025623(20)	7	6	*A*2	7	6	*A*1	*QQ*(7,6,*A*1)	0.0578(4)	−0.00441(25)	0.0626	−0.00483
2199.109277(22)	5	3	*A*2	5	3	*A*1	*QQ*(5,3,*A*1)	0.0643(4)	−0.00503(28)	0.0666	−0.00459
2181.488446(23)	20	3	*A*1	20	3	*A*2	*QQ*(20,3,*A*2)	0.0439(9)		0.0366	−0.00601
2188.854830(50)	19	12	*A*1	19	12	*A*2	*QQ*(19,12,*A*2)	0.0423(5)		0.0432	−0.00583
2190.644817(18)	18	12	*A*1	18	12	*A*2	*QQ*(18,12,*A*2)	0.0455(5)		0.0452	−0.00575
2192.295366(50)	17	12	*A*1	17	12	*A*2	*QQ*(17,12,*A*2)	0.0482(5)		0.0473	−0.00566
2189.941830(15)	15	3	*A*1	15	3	*A*2	*QQ*(15,3,*A*2)	0.0604(6)		0.0479	−0.00565
2195.230195(19)	15	12	*A*1	15	12	*A*2	*QQ*(15,12,*A*2)	0.0451(3)		0.0510	−0.00547
2192.329008(19)	14	6	*A*1	14	6	*A*2	*QQ*(14,6,*A*2)	0.0501(4)	−0.00506(6)	0.0508	−0.00553
2197.729939(10)	13	12	*A*1	13	12	*A*2	*QQ*(13,12,*A*2)	0.0409(2)		0.0503	−0.00546
2193.673797(14)	12	3	*A*1	12	3	*A*2	*QQ*(12,3,*A*2)	0.0618(3)		0.0543	−0.00536
2194.715200(17)	12	6	*A*1	12	6	*A*2	*QQ*(12,6,*A*2)	0.0531(4)	−0.00441(9)	0.0548	−0.00534
2196.820402(16)	12	9	*A*1	12	9	*A*2	*QQ*(12,9,*A*2)	0.0489(3)		0.0559	−0.00526
2194.725295(32)	11	3	*A*1	11	3	*A*2	*QQ*(11,3,*A*2)	0.0601(5)		0.0564	−0.00526
2195.762672(44)	11	6	*A*1	11	6	*A*2	*QQ*(11,6,*A*2)	0.0541(5)	−0.00364(23)	0.0567	−0.00524
2198.015393(18)	11	9	*A*1	11	9	*A*2	*QQ*(11,9,*A*2)	0.0525(5)		0.0574	−0.00516
2198.184821(43)	10	9	*A*1	10	9	*A*2	*QQ*(10,9,*A*2)	0.0508(2)		0.0568	−0.00515
2199.205416(18)	9	9	*A*1	9	9	*A*2	*QQ*(9,9,*A*2)	0.0408(3)	−0.00402(21)	0.0446	−0.00561
2198.344369(36)	8	6	*A*1	8	6	*A*2	*QQ*(8,6,*A*2)	0.0596(4)		0.0621	−0.00490
2198.599351(15)	6	3	*A*1	6	3	*A*2	*QQ*(6,3,*A*2)	0.0601(7)		0.0654	−0.00468
2199.619296(17)	6	6	*A*1	6	6	*A*2	*QQ*(6,6,*A*2)	0.0527(3)	−0.00616(18)	0.0545	−0.00519
2199.532860(24)	4	3	*A*1	4	3	*A*2	*QQ*(4,3,*A*2)	0.0643(7)	−0.00386(20)	0.0676	−0.00450
2199.871121(17)	3	3	*A*1	3	3	*A*2	*QQ*(3,3,*A*2)	0.0650(3)	−0.00541(22)	0.0649	−0.00464
2189.835091(38)	19	13	*E*	19	13	*E*	*QQ*(19,13,*E*)	0.0369(11)		0.0436	−0.00580
2191.619964(15)	18	13	*E*	18	13	*E*	*QQ*(18,13,*E*)	0.0426(15)		0.0457	−0.00571
2192.661323(38)	18	14	*E*	18	14	*E*	*QQ*(18,14,*E*)	0.0413(6)		0.0460	−0.00568
2186.727953(38)	17	2	*E*	17	2	*E*	*QQ*(17,2,*E*)	0.0460(16)		0.0431	−0.00581
2188.444347(38)	17	7	*E*	17	7	*E*	*QQ*(17,7,*E*)	0.0498(13)		0.0451	−0.00577
2194.303984(19)	17	14	*E*	17	14	*E*	*QQ*(17,14,*E*)	0.0335(9)		0.0475	−0.00561
2188.757451(38)	16	4	*E*	16	4	*E*	*QQ*(16,4,*E*)	0.0493(16)		0.0460	−0.00572
2189.106028(37)	16	5	*E*	16	5	*E*	*QQ*(16,5,*E*)	0.0480(14)		0.0464	−0.00572
2190.504296(93)	16	8	*E*	16	8	*E*	*QQ*(16,8,*E*)	0.0414(9)		0.0475	−0.00567
2192.151866(38)	16	10	*E*	16	10	*E*	*QQ*(16,10,*E*)	0.0502(18)		0.0483	−0.00564
2192.939603(15)	16	11	*E*	16	11	*E*	*QQ*(16,11,*E*)	0.0463(15)		0.0488	−0.00561
2194.775123(22)	16	13	*E*	16	13	*E*	*QQ*(16,13,*E*)	0.0416(7)		0.0493	−0.00554

Table 2 (*continued*)

Position[a,b]	J'	K'	N'	J''	K''	N''	Assignment	Measured $\gamma(N_2)$[a,c]	Measured $\delta(N_2)$[a,d]	Calculated $\gamma(N_2)$[c]	Calculated $\delta(N_2)$[c]
2198.036983(43)	16	16	*E*	16	16	*E*	*QQ*(16,16,*E*)	0.0248(9)		0.0260	−0.00624
2189.625404(76)	15	1	*E*	15	1	*E*	*QQ*(15,1,*E*)	0.0566(4)		0.0475	−0.00565
2190.558258(10)	15	5	*E*	15	5	*E*	*QQ*(15,5,*E*)	0.0440(8)		0.0485	−0.00563
2191.474170(78)	15	7	*E*	15	7	*E*	*QQ*(15,7,*E*)	0.0449(11)		0.0491	−0.00560
2193.571946(93)	15	10	*E*	15	10	*E*	*QQ*(15,10,*E*)	0.0469(7)		0.0504	−0.00555
2196.176017(32)	15	13	*E*	15	13	*E*	*QQ*(15,13,*E*)	0.0459(8)	−0.00572(22)	0.0501	−0.00550
2197.188142(59)	15	14	*E*	15	14	*E*	*QQ*(15,14,*E*)	0.0456(9)		0.0457	−0.00565
2191.556757(15)	14	4	*E*	14	4	*E*	*QQ*(14,4,*E*)	0.0472(10)		0.0503	−0.00555
2191.903837(10)	14	5	*E*	14	5	*E*	*QQ*(14,5,*E*)	0.0502(12)		0.0506	−0.00554
2192.822726(19)	14	7	*E*	14	7	*E*	*QQ*(14,7,*E*)	0.0468(18)	−0.00636(20)	0.0511	−0.00552
2193.359300(12)	14	8	*E*	14	8	*E*	*QQ*(14,8,*E*)	0.0481(8)		0.0515	−0.00551
2194.885668(20)	14	10	*E*	14	10	*E*	*QQ*(14,10,*E*)	0.0443(12)		0.0524	−0.00545
2195.666194(29)	14	11	*E*	14	11	*E*	*QQ*(14,11,*E*)	0.0481(8)		0.0527	−0.00540
2197.466314(28)	14	13	*E*	14	13	*E*	*QQ*(14,13,*E*)	0.0401(17)	−0.00668(25)	0.0480	−0.00556
2192.800906(30)	13	4	*E*	13	4	*E*	*QQ*(13,4,*E*)	0.0527(11)	−0.00453(26)	0.0524	−0.00546
2193.149071(18)	13	5	*E*	13	5	*E*	*QQ*(13,5,*E*)	0.0549(8)	−0.00844(22)	0.0526	−0.00545
2194.066411(16)	13	7	*E*	13	7	*E*	*QQ*(13,7,*E*)	0.0505(11)	−0.00304(6)	0.0531	−0.00543
2194.614362(15)	13	8	*E*	13	8	*E*	*QQ*(13,8,*E*)	0.0512(8)		0.0535	−0.00541
2196.096792(24)	13	10	*E*	13	10	*E*	*QQ*(13,10,*E*)	0.0495(8)	−0.00549(22)	0.0543	−0.00534
2196.872853(12)	13	11	*E*	13	11	*E*	*QQ*(13,11,*E*)	0.0499(9)	−0.00610(16)	0.0539	−0.00533
2193.481684(55)	12	2	*E*	12	2	*E*	*QQ*(12,2,*E*)	0.0493(10)	−0.00598(24)	0.0542	−0.00537
2193.946191(15)	12	4	*E*	12	4	*E*	*QQ*(12,4,*E*)	0.0552(6)	−0.00442(16)	0.0544	−0.00536
2195.209488(12)	12	7	*E*	12	7	*E*	*QQ*(12,7,*E*)	0.0532(8)	−0.00537(25)	0.0550	−0.00533
2197.981144(10)	12	11	*E*	12	11	*E*	*QQ*(12,11,*E*)	0.0458(19)		0.0525	−0.00536
2194.532634(34)	11	2	*E*	11	2	*E*	*QQ*(11,2,*E*)	0.0512(9)	−0.00489(21)	0.0563	−0.00526
2194.995471(15)	11	4	*E*	11	4	*E*	*QQ*(11,4,*E*)	0.0576(8)	−0.00332(23)	0.0564	−0.00525
2195.340883(11)	11	5	*E*	11	5	*E*	*QQ*(11,5,*E*)	0.0557(12)	−0.00505(10)	0.0565	−0.00524
2196.255517(82)	11	7	*E*	11	7	*E*	*QQ*(11,7,*E*)	0.0543(12)	−0.00561(13)	0.0570	−0.00523
2196.813464(18)	11	8	*E*	11	8	*E*	*QQ*(11,8,*E*)	0.0558(9)		0.0574	−0.00519
2198.224819(75)	11	10	*E*	11	10	*E*	*QQ*(11,10,*E*)	0.0479(9)		0.0547	−0.00526
2195.488911(21)	10	2	*E*	10	2	*E*	*QQ*(10,2,*E*)	0.0599(3)	−0.00420(28)	0.0584	−0.00514
2196.294520(80)	10	5	*E*	10	5	*E*	*QQ*(10,5,*E*)	0.0592(5)	−0.00430(18)	0.0584	−0.00513
2197.206975(11)	10	7	*E*	10	7	*E*	*QQ*(10,7,*E*)	0.0569(5)		0.0590	−0.00511
2197.766867(70)	10	8	*E*	10	8	*E*	*QQ*(10,8,*E*)	0.0526(3)	−0.00516(3)	0.0590	−0.00508
2199.148473(32)	10	10	*E*	10	10	*E*	*QQ*(10,10,*E*)	0.0348(7)	−0.00551(29)	0.0416	−0.00573
2196.353188(29)	9	2	*E*	9	2	*E*	*QQ*(9,2,*E*)	0.0620(16)		0.0604	−0.00502
2197.156293(11)	9	5	*E*	9	5	*E*	*QQ*(9,5,*E*)	0.0595(6)		0.0603	−0.00503
2198.065301(48)	9	7	*E*	9	7	*E*	*QQ*(9,7,*E*)	0.0568(4)	−0.00584(29)	0.0606	−0.00499
2197.012526(57)	8	1	*E*	8	1	*E*	*QQ*(8,1,*E*)	0.0585(4)		0.0624	−0.00489
2197.127502(17)	8	2	*E*	8	2	*E*	*QQ*(8,2,*E*)	0.0646(4)		0.0624	−0.00490
2197.585066(15)	8	4	*E*	8	4	*E*	*QQ*(8,4,*E*)	0.0601(3)	−0.00441(29)	0.0620	−0.00491
2197.927650(62)	8	5	*E*	8	5	*E*	*QQ*(8,5,*E*)	0.0592(7)		0.0620	−0.00492
2199.396986(26)	8	8	*E*	8	8	*E*	*QQ*(8,8,*E*)	0.0430(7)	−0.00619(20)	0.0478	−0.00548
2197.698394(37)	7	1	*E*	7	1	*E*	*QQ*(7,1,*E*)	0.0601(5)		0.0644	−0.00476
2197.810939(11)	7	2	*E*	7	2	*E*	*QQ*(7,2,*E*)	0.0677(6)		0.0642	−0.00477
2198.268055(51)	7	4	*E*	7	4	*E*	*QQ*(7,4,*E*)	0.0619(4)	−0.00428(18)	0.0636	−0.00481
2199.514462(29)	7	7	*E*	7	7	*E*	*QQ*(7,7,*E*)	0.0480(3)	−0.00489(27)	0.0511	−0.00534
2198.294879(10)	6	1	*E*	6	1	*E*	*QQ*(6,1,*E*)	0.0697(7)		0.0663	−0.00462
2198.409985(31)	6	2	*E*	6	2	*E*	*QQ*(6,2,*E*)	0.0652(8)		0.0659	−0.00465
2199.372836(28)	5	4	*E*	5	4	*E*	*QQ*(5,4,*E*)	0.0646(3)	−0.00314(13)	0.0660	−0.00461
2199.713163(21)	5	5	*E*	5	5	*E*	*QQ*(5,5,*E*)	0.0565(6)	−0.00509(21)	0.0579	−0.00502
2199.229001(75)	4	1	*E*	4	1	*E*	*QQ*(4,1,*E*)	0.0675(3)	−0.00279(21)	0.0692	−0.00439
2199.795950(23)	4	4	*E*	4	4	*E*	*QQ*(4,4,*E*)	0.0608(4)	−0.00528(29)	0.0614	−0.00484
2199.568878(59)	3	1	*E*	3	1	*E*	*QQ*(3,1,*E*)	0.0645(3)		0.0704	−0.00430
2199.682385(23)	3	2	*E*	3	2	*E*	*QQ*(3,2,*E*)	0.0663(2)	−0.00218(7)	0.0693	−0.00438
2199.822489(17)	2	1	*E*	2	1	*E*	*QQ*(2,1,*E*)	0.0657(11)	−0.00085(11)	0.0715	−0.00423
2199.935691(13)	2	2	*E*	2	2	*E*	*QQ*(2,2,*E*)	0.0669(5)		0.0684	−0.00443
2199.991040(37)	1	1	*E*	1	1	*E*	*QQ*(1,1,*E*)	0.0664(8)	−0.00218(28)	0.0718	−0.00421
2317.474656(17)	17	0	*A*2	16	0	*A*1	*QR*(16,0,*A*1)	0.0478(4)		0.0454	−0.00569
2311.769515(25)	16	3	*A*2	15	3	*A*1	*QR*(15,3,*A*1)	0.0554(2)		0.0488	−0.00558
2305.603182(26)	15	3	*A*2	14	3	*A*1	*QR*(14,3,*A*1)	0.0547(4)		0.0509	−0.00547
2299.325006(26)	14	3	*A*2	13	3	*A*1	*QR*(13,3,*A*1)	0.0580(2)	−0.00497(25)	0.0530	−0.00536
2302.163126(98)	14	9	*A*2	13	9	*A*1	*QR*(13,9,*A*1)	0.0498(5)	−0.00263(6)	0.0557	−0.00506

(*continued on next page*)

Table 2 (*continued*)

Position[a,b]	J'	K'	N'	J''	K''	N''	Assignment	Measured $\gamma(N_2)$[a,c]	Measured $\delta(N_2)$[a,d]	Calculated $\gamma(N_2)$[c]	Calculated $\delta(N_2)$[c]
2292.605372(49)	13	0	*A*2	12	0	*A*1	*QR*(12,0,*A*1)	0.0615(7)	−0.00389(9)	0.0540	−0.00528
2295.793364(86)	13	9	*A*2	12	9	*A*1	*QR*(12,9,*A*1)	0.0505(4)	−0.00448(10)	0.0568	−0.00488
2287.371726(29)	12	6	*A*2	11	6	*A*1	*QR*(11,6,*A*1)	0.0531(7)	−0.00524(20)	0.0590	−0.00494
2289.343681(60)	12	9	*A*2	11	9	*A*1	*QR*(11,9,*A*1)	0.0569(7)		0.0575	−0.00463
2279.463137(20)	11	0	*A*2	10	0	*A*1	*QR*(10,0,*A*1)	0.0611(6)		0.0581	−0.00502
2279.786350(23)	11	3	*A*2	10	3	*A*1	*QR*(10,3,*A*1)	0.0541(5)	−0.00421(23)	0.0592	−0.00497
2280.749132(17)	11	6	*A*2	10	6	*A*1	*QR*(10,6,*A*1)	0.0541(4)		0.0606	−0.00477
2282.879526(34)	11	9	*A*2	10	9	*A*1	*QR*(10,9,*A*1)	0.0542(3)	−0.00554(9)	0.0578	−0.00430
2273.053106(16)	10	3	*A*2	9	3	*A*1	*QR*(9,3,*A*1)	0.0545(3)	−0.00473(16)	0.0612	−0.00481
2274.018828(17)	10	6	*A*2	9	6	*A*1	*QR*(9,6,*A*1)	0.0565(2)	−0.00448(25)	0.0620	−0.00459
2275.377085(48)	10	9	*A*2	9	9	*A*1	*QR*(9,9,*A*1)	0.0605(6)	−0.00691(15)	0.0573	−0.00380
2265.890262(70)	9	0	*A*2	8	0	*A*1	*QR*(8,0,*A*1)	0.0624(2)	−0.00309(4)	0.0621	−0.00472
2266.215383(12)	9	3	*A*2	8	3	*A*1	*QR*(8,3,*A*1)	0.0540(3)	−0.00484(14)	0.0631	−0.00463
2267.184143(15)	9	6	*A*2	8	6	*A*1	*QR*(8,6,*A*1)	0.0606(4)	−0.00407(25)	0.0629	−0.00439
2259.275683(16)	8	3	*A*2	7	3	*A*1	*QR*(7,3,*A*1)	0.0584(3)	−0.00442(26)	0.0650	−0.00444
2260.247875(20)	8	6	*A*2	7	6	*A*1	*QR*(7,6,*A*1)	0.0630(3)		0.0629	−0.00416
2251.910504(16)	7	0	*A*2	6	0	*A*1	*QR*(6,0,*A*1)	0.0656(5)	−0.00458(2)	0.0659	−0.00435
2252.237807(13)	7	3	*A*2	6	3	*A*1	*QR*(6,3,*A*1)	0.0631(3)	−0.00433(14)	0.0666	−0.00427
2245.102240(13)	6	3	*A*2	5	3	*A*1	*QR*(5,3,*A*1)	0.0636(5)	−0.00451(11)	0.0679	−0.00414
2237.543698(23)	5	0	*A*2	4	0	*A*1	*QR*(4,0,*A*1)	0.0661(4)	−0.00379(2)	0.0692	−0.00406
2230.551914(14)	4	3	*A*2	3	3	*A*1	*QR*(3,3,*A*1)	0.0710(5)	−0.00283(25)	0.0667	−0.00383
2222.806716(12)	3	0	*A*2	2	0	*A*1	*QR*(2,0,*A*1)	0.0674(4)	−0.00329(14)	0.0713	−0.00397
2207.713981(15)	1	0	*A*2	0	0	*A*1	*QR*(0,0,*A*1)	0.0679(5)			
2317.796500(23)	17	3	*A*1	16	3	*A*2	*QR*(16,3,*A*2)	0.0545(3)		0.0466	−0.00568
2311.446204(17)	16	0	*A*1	15	0	*A*2	*QR*(15,0,*A*2)	0.0506(3)		0.0476	−0.00560
2311.757892(16)	16	3	*A*1	15	3	*A*2	*QR*(15,3,*A*2)	0.0554(2)		0.0488	−0.00558
2312.703179(33)	16	6	*A*1	15	6	*A*2	*QR*(15,6,*A*2)	0.0529(3)	−0.00816(21)	0.0513	−0.00544
2314.568396(26)	16	9	*A*1	15	9	*A*2	*QR*(15,9,*A*2)	0.0431(7)		0.0529	−0.00531
2305.610445(21)	15	3	*A*1	14	3	*A*2	*QR*(14,3,*A*2)	0.0547(4)		0.0509	−0.00547
2306.553783(84)	15	6	*A*1	14	6	*A*2	*QR*(14,6,*A*2)	0.0488(7)		0.0533	−0.00533
2308.429504(39)	15	9	*A*1	14	9	*A*2	*QR*(14,9,*A*2)	0.0473(8)		0.0544	−0.00519
2310.405392(45)	15	12	*A*1	14	12	*A*2	*QR*(14,12,*A*2)	0.0426(5)		0.0522	−0.00481
2299.006264(43)	14	0	*A*1	13	0	*A*2	*QR*(13,0,*A*2)	0.0602(4)		0.0519	−0.00539
2300.278432(44)	14	6	*A*1	13	6	*A*2	*QR*(13,6,*A*2)	0.0512(5)	−0.00492(20)	0.0553	−0.00521
2293.882895(43)	13	6	*A*1	12	6	*A*2	*QR*(12,6,*A*2)	0.0522(2)	−0.00503(26)	0.0572	−0.00509
2286.089730(55)	12	0	*A*1	11	0	*A*2	*QR*(11,0,*A*2)	0.0601(5)	−0.00342(14)	0.0561	−0.00515
2286.411835(51)	12	3	*A*1	11	3	*A*2	*QR*(11,3,*A*2)	0.0542(5)	−0.00441(23)	0.0572	−0.00511
2272.729320(22)	10	0	*A*1	9	0	*A*2	*QR*(9,0,*A*2)	0.0620(5)		0.0602	−0.00488
2258.949908(20)	8	0	*A*1	7	0	*A*2	*QR*(7,0,*A*2)	0.0637(7)		0.0641	−0.00454
2253.213050(15)	7	6	*A*1	6	6	*A*2	*QR*(6,6,*A*2)	0.0635(3)		0.0614	−0.00383
2244.774291(16)	6	0	*A*1	5	0	*A*2	*QR*(5,0,*A*2)	0.0648(6)		0.0677	−0.00418
2237.873620(18)	5	3	*A*1	4	3	*A*2	*QR*(4,3,*A*2)	0.0664(4)	−0.00356(16)	0.0685	−0.00395
2230.220468(16)	4	0	*A*1	3	0	*A*2	*QR*(3,0,*A*2)	0.0656(2)		0.0704	−0.00403
2215.303960(15)	2	0	*A*1	1	0	*A*2	*QR*(1,0,*A*2)	0.0681(3)	−0.00250(22)	0.0718	−0.00382
2317.511311(18)	17	1	*E*	16	1	*E*	*QR*(16,1,*E*)	0.0535(9)		0.0456	−0.00570
2317.614865(12)	17	2	*E*	16	2	*E*	*QR*(16,2,*E*)	0.0525(9)		0.0460	−0.00570
2311.480485(14)	16	1	*E*	15	1	*E*	*QR*(15,1,*E*)	0.0546(9)	−0.00465(24)	0.0478	−0.00561
2311.587024(17)	16	2	*E*	15	2	*E*	*QR*(15,2,*E*)	0.0566(9)	−0.00940(21)	0.0482	−0.00560
2312.008763(45)	16	4	*E*	15	4	*E*	*QR*(15,4,*E*)	0.0557(16)	−0.00550(29)	0.0496	−0.00554
2312.322600(21)	16	5	*E*	15	5	*E*	*QR*(15,5,*E*)	0.0535(8)		0.0504	−0.00549
2313.570034(50)	16	8	*E*	15	8	*E*	*QR*(15,8,*E*)	0.0411(13)		0.0527	−0.00535
2305.429811(11)	15	2	*E*	14	2	*E*	*QR*(14,2,*E*)	0.0585(9)	−0.00932(24)	0.0503	−0.00550
2305.853834(12)	15	4	*E*	14	4	*E*	*QR*(14,4,*E*)	0.0534(16)	−0.00731(8)	0.0517	−0.00543
2306.997511(56)	15	7	*E*	14	7	*E*	*QR*(14,7,*E*)	0.0483(13)		0.0540	−0.00528
2307.461159(32)	15	8	*E*	14	8	*E*	*QR*(14,8,*E*)	0.0460(15)	−0.00859(22)	0.0544	−0.00524
2308.909301(20)	15	10	*E*	14	10	*E*	*QR*(14,10,*E*)	0.0443(14)		0.0540	−0.00514
2299.041634(11)	14	1	*E*	13	1	*E*	*QR*(13,1,*E*)	0.0615(9)	−0.00278(3)	0.0521	−0.00540
2299.148707(57)	14	2	*E*	13	2	*E*	*QR*(13,2,*E*)	0.0591(16)	−0.00656(17)	0.0524	−0.00539
2299.574610(63)	14	4	*E*	13	4	*E*	*QR*(13,4,*E*)	0.0557(14)	−0.00419(14)	0.0538	−0.00532
2299.892556(68)	14	5	*E*	13	5	*E*	*QR*(13,5,*E*)	0.0525(9)	−0.00608(22)	0.0546	−0.00527
2300.727775(12)	14	7	*E*	13	7	*E*	*QR*(13,7,*E*)	0.0475(18)	−0.00617(41)	0.0558	−0.00516
2301.212629(16)	14	8	*E*	13	8	*E*	*QR*(13,8,*E*)	0.0491(15)	−0.00735(30)	0.0560	−0.00511
2303.323274(22)	14	11	*E*	13	11	*E*	*QR*(13,11,*E*)	0.0449(10)		0.0539	−0.00476
2292.640893(55)	13	1	*E*	12	1	*E*	*QR*(12,1,*E*)	0.0598(12)	−0.00058(3)	0.0542	−0.00528

Table 2 (*continued*)

Position[a,b]	J'	K'	N'	J''	K''	N''	Assignment	Measured $\gamma(N_2)$[a,c]	Measured $\delta(N_2)$[a,d]	Calculated $\gamma(N_2)$[c]	Calculated $\delta(N_2)$[c]
2292.748283(55)	13	2	*E*	12	2	*E*	*QR*(12,2,*E*)	0.0591(8)	−0.00614(24)	0.0545	−0.00527
2293.175836(59)	13	4	*E*	12	4	*E*	*QR*(12,4,*E*)	0.0546(17)	−0.00616(28)	0.0559	−0.00519
2293.495069(64)	13	5	*E*	12	5	*E*	*QR*(12,5,*E*)	0.0532(9)	−0.00521(29)	0.0566	−0.00514‘
2294.335703(11)	13	7	*E*	12	7	*E*	*QR*(12,7,*E*)	0.0506(8)	−0.00630(13)	0.0575	−0.00503
2294.835594(11)	13	8	*E*	12	8	*E*	*QR*(12,8,*E*)	0.0509(11)	−0.00789(19)	0.0574	−0.00497
2296.201942(18)	13	10	*E*	12	10	*E*	*QR*(12,10,*E*)	0.0533(7)	−0.00585(25)	0.0557	−0.00469
2296.911173(27)	13	11	*E*	12	11	*E*	*QR*(12,11,*E*)	0.0466(11)		0.0546	−0.00437
2286.125439(85)	12	1	*E*	11	1	*E*	*QR*(11,1,*E*)	0.0609(8)	−0.00088(7)	0.0562	−0.00516
2286.233086(35)	12	2	*E*	11	2	*E*	*QR*(11,2,*E*)	0.0593(8)	−0.00549(23)	0.0566	−0.00514
2286.661999(37)	12	4	*E*	11	4	*E*	*QR*(11,4,*E*)	0.0558(9)	−0.00441(21)	0.0579	−0.00506
2286.982296(40)	12	5	*E*	11	5	*E*	*QR*(11,5,*E*)	0.0566(13)	−0.00588(25)	0.0585	−0.00500
2287.827430(77)	12	7	*E*	11	7	*E*	*QR*(11,7,*E*)	0.0526(10)	−0.00410(21)	0.0590	−0.00487
2288.337961(60)	12	8	*E*	11	8	*E*	*QR*(11,8,*E*)	0.0549(12)	−0.00551(23)	0.0585	−0.00479
2289.674530(13)	12	10	*E*	11	10	*E*	*QR*(11,10,*E*)	0.0565(18)		0.0562	−0.00434
2290.384543(19)	12	11	*E*	11	11	*E*	*QR*(11,11,*E*)	0.0499(8)		0.0548	−0.00376
2279.499010(20)	11	1	*E*	10	1	*E*	*QR*(10,1,*E*)	0.0613(8)	−0.00398(7)	0.0583	−0.00503
2279.607057(20)	11	2	*E*	10	2	*E*	*QR*(10,2,*E*)	0.0597(8)	−0.00536(25)	0.0587	−0.00501
2280.037073(21)	11	4	*E*	10	4	*E*	*QR*(10,4,*E*)	0.0556(19)	−0.00398(26)	0.0598	−0.00491
2280.358295(29)	11	5	*E*	10	5	*E*	*QR*(10,5,*E*)	0.0546(8)		0.0604	−0.00484
2281.207316(29)	11	7	*E*	10	7	*E*	*QR*(10,7,*E*)	0.0553(11)		0.0603	−0.00469
2281.725171(36)	11	8	*E*	10	8	*E*	*QR*(10,8,*E*)	0.0569(8)		0.0593	−0.00456
2283.036952(71)	11	10	*E*	10	10	*E*	*QR*(10,10,*E*)	0.0614(11)		0.0560	−0.00378
2272.763995(22)	10	1	*E*	9	1	*E*	*QR*(9,1,*E*)	0.0638(9)	−0.00296(3)	0.0603	−0.00488
2272.873144(21)	10	2	*E*	9	2	*E*	*QR*(9,2,*E*)	0.0599(9)	−0.00551(20)	0.0607	−0.00486
2273.304509(20)	10	4	*E*	9	4	*E*	*QR*(9,4,*E*)	0.0558(7)	−0.00420(22)	0.0618	−0.00474
2273.626567(21)	10	5	*E*	9	5	*E*	*QR*(9,5,*E*)	0.0573(10)	−0.00478(29)	0.0621	−0.00467
2274.479063(28)	10	7	*E*	9	7	*E*	*QR*(9,7,*E*)	0.0597(6)	−0.00416(23)	0.0611	−0.00447
2275.002779(36)	10	8	*E*	9	8	*E*	*QR*(9,8,*E*)	0.0612(7)	−0.00261(5)	0.0595	−0.00426
2265.925426(16)	9	1	*E*	8	1	*E*	*QR*(8,1,*E*)	0.0636(7)	−0.00411(4)	0.0623	−0.00472
2266.034928(16)	9	2	*E*	8	2	*E*	*QR*(8,2,*E*)	0.0608(10)	−0.00484(25)	0.0626	−0.00469
2266.467560(17)	9	4	*E*	8	4	*E*	*QR*(8,4,*E*)	0.0586(9)	−0.00452(29)	0.0636	−0.00456
2266.790714(18)	9	5	*E*	8	5	*E*	*QR*(8,5,*E*)	0.0592(8)	−0.00426(29)	0.0636	−0.00448
2267.646358(25)	9	7	*E*	8	7	*E*	*QR*(8,7,*E*)	0.0627(12)	−0.00238(1)	0.0612	−0.00421
2268.174445(40)	9	8	*E*	8	8	*E*	*QR*(8,8,*E*)	0.0573(12)		0.0586	−0.00382
2258.986191(21)	8	1	*E*	7	1	*E*	*QR*(7,1,*E*)	0.0626(5)	−0.00426(4)	0.0642	−0.00453
2259.095017(20)	8	2	*E*	7	2	*E*	*QR*(7,2,*E*)	0.0602(3)	−0.00489(24)	0.0646	−0.00450
2259.528937(21)	8	4	*E*	7	4	*E*	*QR*(7,4,*E*)	0.0606(5)	−0.00444(27)	0.0651	−0.00437
2259.853196(23)	8	5	*E*	7	5	*E*	*QR*(7,5,*E*)	0.0621(5)		0.0646	−0.00430
2260.712073(36)	8	7	*E*	7	7	*E*	*QR*(7,7,*E*)	0.0702(3)		0.0599	−0.00383
2251.945889(17)	7	1	*E*	6	1	*E*	*QR*(6,1,*E*)	0.0656(7)	−0.00347(3)	0.0661	−0.00434
2252.056150(16)	7	2	*E*	6	2	*E*	*QR*(6,2,*E*)	0.0616(16)	−0.00440(24)	0.0664	−0.00431
2252.491620(18)	7	4	*E*	6	4	*E*	*QR*(6,4,*E*)	0.0644(6)	−0.00420(26)	0.0663	−0.00421
2252.816887(20)	7	5	*E*	6	5	*E*	*QR*(6,5,*E*)	0.0664(6)	−0.00286(27)	0.0648	−0.00411
2244.809883(15)	6	1	*E*	5	1	*E*	*QR*(5,1,*E*)	0.0657(5)	−0.00282(2)	0.0678	−0.00418
2244.920370(16)	6	2	*E*	5	2	*E*	*QR*(5,2,*E*)	0.0625(3)	−0.00491(22)	0.0680	−0.00417
2245.357740(18)	6	4	*E*	5	4	*E*	*QR*(5,4,*E*)	0.0688(7)	−0.00374(28)	0.0666	−0.00404
2245.684167(21)	6	5	*E*	5	5	*E*	*QR*(5,5,*E*)	0.0720(7)	−0.00203(5)	0.0629	−0.00383
2237.580370(23)	5	1	*E*	4	1	*E*	*QR*(4,1,*E*)	0.0656(4)	−0.00188(3)	0.0692	−0.00408
2237.690483(23)	5	2	*E*	4	2	*E*	*QR*(4,2,*E*)	0.0641(3)	−0.00348(22)	0.0693	−0.00408
2238.129466(32)	5	4	*E*	4	4	*E*	*QR*(4,4,*E*)	0.0737(4)	−0.00074(4)	0.0647	−0.00383
2230.256562(16)	4	1	*E*	3	1	*E*	*QR*(3,1,*E*)	0.0656(5)	−0.00034(3)	0.0705	−0.00403
2230.367954(16)	4	2	*E*	3	2	*E*	*QR*(3,2,*E*)	0.0661(6)	−0.00419(24)	0.0702	−0.00387
2222.842099(12)	3	1	*E*	2	1	*E*	*QR*(2,1,*E*)	0.0674(5)	−0.00033(1)	0.0714	−0.00386
2222.954864(13)	3	2	*E*	2	2	*E*	*QR*(2,2,*E*)	0.0709(8)	−0.00445(20)	0.0690	−0.00377
2215.341208(31)	2	1	*E*	1	1	*E*	*QR*(1,1,*E*)	0.0684(6)	−0.00338(21)	0.0714	−0.00363

$J'' = K$ and $J'' = K + 1$ in the ^{Q}Q-branch, were fitted to the following expression:

$$\gamma(N_2) = c_0 + c_1|m|(|m| + 1) + c_2K^2. \quad (1)$$

$\gamma(N_2)$ is expressed in $cm^{-1}\,atm^{-1}$ at 296 K. The constants c_0, c_1, and c_2 were determined by a least-squares fit to the present measured broadening coefficients and are given in Table 4. For the fit with 346 lines, the average percentage

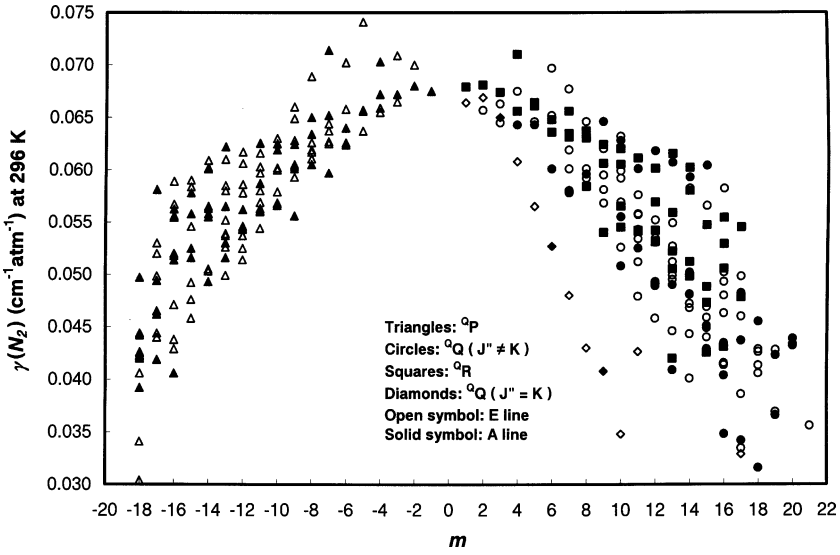

Fig. 2. Measured N_2-broadening coefficients, $\gamma(N_2)$, (cm^{-1} atm^{-1} at 296 K) in the ^{Q}P-, ^{Q}Q- and ^{Q}R-branches as a function of m. The $J'' = K$ transitions in the ^{Q}Q-branch are plotted with diamond symbols highlighting the rapidly falling trend of the corresponding N_2-broadening coefficients with m.

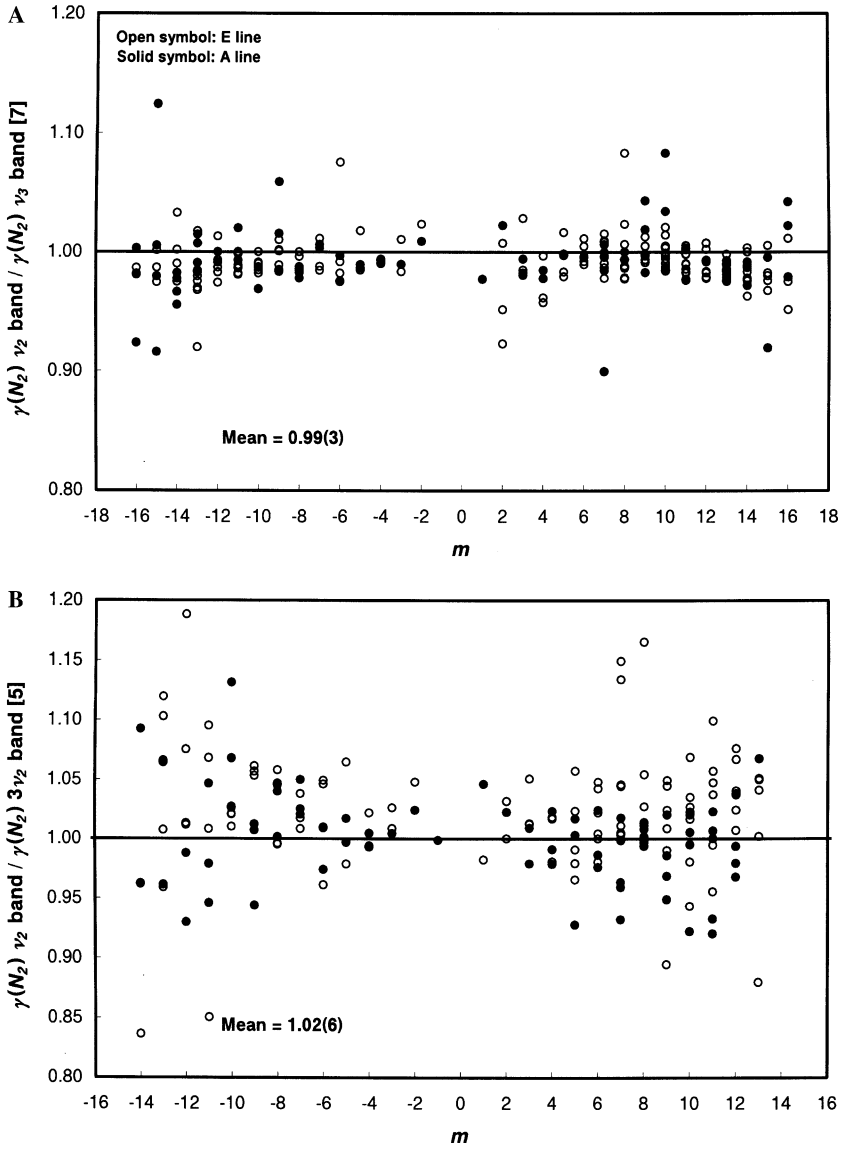

Fig. 3. Comparisons between the N_2-broadening coefficients obtained in the present study and those obtained by (A) Devi et al. [7] and (B) Boussin et al. [5].

Table 3
Comparison of present and previous N_2-broadened halfwidth measurements

Reference	Band	Mean ratio of $\gamma(N_2)$ present work/$\gamma(N_2)$ previous studies[a]	Percentage of lines compared
Chudamani and Varanasi [17]	v_2	1.02(4)	4
Devi et al. [7]	v_3	0.99(3)	245
Blanquet at al. [14]	v_3	1.02(3)	33
Boussin et al. [5]	$3v_2$	1.02(6)	183

[a] The values in parentheses represent one standard deviation uncertainties in the measured quantities in units of the last quoted digit.

Table 4
Coefficients for the empirical expansions of the broadening parameters (Eqs. (1) and (2)) in the v_2 and v_3 bands

All ^QP and ^QR transitions, and ^QQ transitions with $J'' \neq K$			^QQ transitions with $J'' = K$		^QQ transitions with $J'' = K+1$
Band	v_2	v_3	v_2	v_3	v_2
c_0	0.0674(4)	0.0679(4)	0.0684(5)	0.0700(9)	0.0680(6)
c_1	$-5.51(21)\times10^{-5}$	$-4.\ 98(30)\times10^{-5}$	$-4.03(13)\times10^{-4}$	$-4.26(19)\times10^{-4}$	$-1.80(12)\times10^{-4}$
c_2	$-6.25(48)\times10^{-5}$	$-7.96(65)\times10^{-5}$	$8.94(48)\times10^{-7}$	$9.93(78)\times10^{-7}$	$2.14(47)\times10^{-7}$
RMS error	3.9%	6.3%	1.06%	3.4%	1.12%
#lines	346	297	11	13	10

The values for the coefficients in the v_3 band are taken from [7].
The values in parentheses represent one standard deviation uncertainties in the measured quantities in units of the last quoted digit.

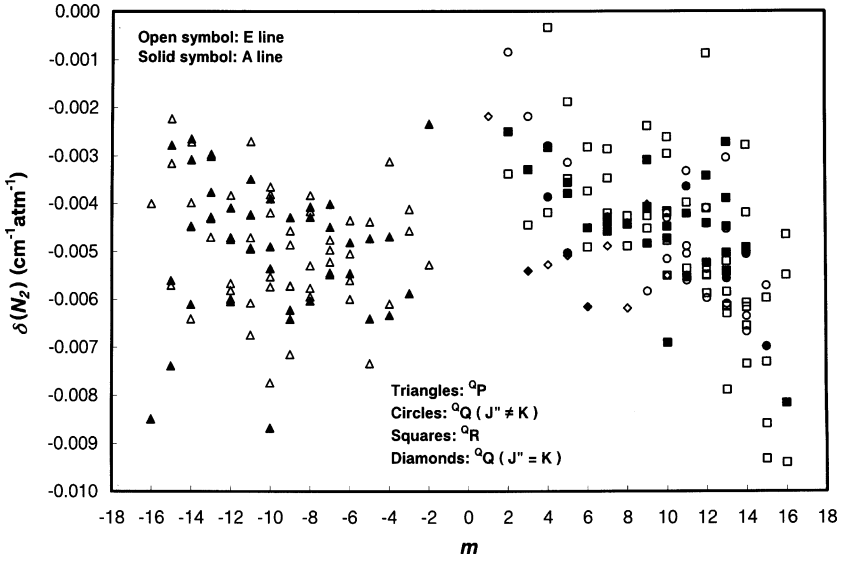

Fig. 4. Measured N_2-induced pressure-shift coefficients, $\delta(N_2)$, (cm^{-1} atm^{-1} at the temperature of the spectra) as a function of m.

difference between the experimental and calculated broadening coefficients (using Eq. (1) and parameters in Table 4) is 4.4%.

In the ^QQ branch for the $J'' = K$ transitions the broadening coefficients were expressed as

$$\gamma = c_0 + c_1|m|(|m|+1) + c_2|m|^2(|m|+1)^2. \quad (2)$$

As again determined by a least-squares fit to the data, the constants c_0, c_1, and c_2 are also given in Table 4. The percentage difference between the experimental and calculated broadening coefficients (using Eq. (2) and parameters in Table 4) for the fit with 11 transitions is 1.33%.

We noticed that the ^QQ branch transitions with the $J'' = K+1$ also follow a distinctive pattern and have fitted them to Eq. (2). The c_0, c_1, and c_2 constants for this last fit are also given in Table 4. Overall, on average the empirical expressions reproduce the measured broadening coefficients to 4.7%.

3.2. Discussion of the measured N_2-induced pressure-shift coefficients

All of our measured pressure-induced N_2-shift coefficients, $\delta(N_2)$, in Table 2 are between -0.009 and $0\ cm^{-1}$. The measured pressure-shift coefficients have been plotted as a function of m in Fig. 4. The N_2-induced pressure-shift coefficients for ^QQ-branch $J'' = K$ transitions are smaller than shifts with the same m value but different K values. This trend is not as clearly defined as it is for N_2-broadening coefficients, though (see Fig. 2).

4. Theoretical modeling of broadening and shift coefficients

4.1. General formulation

In this study, we have assumed that CH_3D behaves like a linear molecule for its interaction with N_2. Then, the N_2-broadening and shifting coefficients are calculated on the basis of the semiclassical Robert and Bonamy (RB) model [20]. Within this model, the broadening coefficient γ and pressure-shift coefficient δ of an isolated pressure-broadened rotational or rovibrational $i \to f$ line ($v_i J_i K_i \to v_f J_f K_f$) may be expressed as

$$\gamma - i\delta = \frac{n_2 \bar{v}}{2\pi c} \sum_{J_2} \rho_{J_2} \int_0^\infty 2\pi b S_{if}(b, J_2)\, db, \tag{3}$$

where n_2 is the number density of the perturbing molecules, $\bar{v}$ is the mean relative speed, ρ_{J_2} is the relative population of the perturber in the $|J_2, v_2 = 0\rangle$ state including the nuclear spin factor $f(J_2) = (-1)^{J_2} + 3$, S_{if} is the complex differential cross-section ($S_{if} = S^b - iS^s$) representing the collisional efficiency, and b is the impact parameter. Within the RB formalism [20], the differential broadening and shift cross-sections S^b and S^s are given by

$$S^b(b) = 1 - \exp\left[-\mathrm{Re}\, S_2^{\mathrm{aniso}}(b)\right] \cos\left[\mathrm{Im}\, S_2^{\mathrm{aniso}}(b) + S_1^{\mathrm{iso}}(b)\right], \tag{4}$$

$$S^s(b) = \exp\left[-\mathrm{Re}\, S_2^{\mathrm{aniso}}(b)\right] \sin\left[\mathrm{Im}\, S_2^{\mathrm{aniso}}(b) + S_1^{\mathrm{iso}}(b)\right], \tag{5}$$

where S_2^{aniso} is derived from the anisotropic part of the potential and represents the second-order perturbation expansion of $S(b)$; $\mathrm{Im}\, S_2^{\mathrm{aniso}}(b)$ results from the noncommutative character of the interaction at two different times; $S_1^{\mathrm{iso}}(b)$ is the vibrational phase shift arising from the difference in the isotropic part of the potential V_{iso}, between the initial and final state of the transition. The various contributions to S_2^{aniso} are given with a good approximation by Leavitt and Korff [25] as

$$S_2^{\mathrm{aniso}} = \sum_{l_1, l_2} {}^{l_1 l_2} S_{2,i}^{\mathrm{outer}} + {}^{l_1 l_2} S_{2,f}^{\mathrm{outer}} + {}^{l_1 l_2} S_2^{\mathrm{middle}}, \tag{6}$$

where $S_{2,i}^{\mathrm{outer}}$, $S_{2,f}^{\mathrm{outer}}$, S_2^{middle} are the second-order terms of the perturbation development of S_{if} and l_1, l_2 represent the orders of the spherical harmonics considered for the absorber and the perturber (in this calculation the total order $l_1 + l_2$ is limited to 4 for the atom–atom potential).

Assuming that the three hydrogen atoms (noted as $_3$H) of CH_3D are situated at the position of their projection in the C–D axis, the intermolecular potential V_T used involves, in addition to the electrostatic interactions V_e, the atom–atom Lennard-Jones (LJ) model V_{aa} such that

$$V_T = V_{\Omega_1 Q_2} + V_{\Omega_1 \Phi_2} + V_{\Phi_1 Q_2} + V_{\Phi_1 \Phi_2} + \sum_{i,j} 4\varepsilon_{ij} \left[\left(\frac{\sigma_{ij}}{r_{ij}}\right)^{12} - \left(\frac{\sigma_{ij}}{r_{ij}}\right)^{6} \right], \tag{7}$$

where the index 1 refers to the absorber (CH_3D) and the index 2 to the perturber (N_2); Q, Ω, and Φ are the quadrupole, octopole, and hexadecapole moments of molecules (note that we have neglected the very weak dipole [26] and quadrupole moments of CH_3D); ε_{ij} and σ_{ij} are the LJ parameters for the interaction of the ith atom for molecule 1 ($_3$H, C, and D) and jth atom for molecule 2, and r_{ij} is the distance between these atoms. By expanding r_{ij} in power series of the intermolecular distance r, V_T can be expressed in terms of the spherical harmonics considered for each molecule and the intramolecular distances r_{1i} of $_3\mathrm{H} \equiv$ C–D and r_{2j} of N–N of each atom i or j to their mass center.

The trajectory model [27] includes the influence of the isotropic potential in energy conservation and in the equation of motion around the distance of closest approach r_c. The actual trajectory is replaced by an equivalent straight-line trajectory described at the velocity v_c'. The LJ parameters $_3$H–$_3$H, C–C, and D–D for $_3$HCD–$_3$HCD interactions were evaluated previously [22]. For N_2, we have considered the exact LJ parameters derived from experimental values of second virial coefficients $B(T)$ in the temperature range 200–500 K [28]. The parameters $_3$H–N, C–N, and D–N for $_3$HCD–N_2 interactions are obtained using the usual mixing rules $\sigma_{ij} = (\sigma_{ii} + \sigma_{jj})/2$ and $\varepsilon_{ij} = (\varepsilon_{ii}\varepsilon_{jj})^{1/2}$. The rotational constants B and D used for the v_2 band of CH_3D were evaluated previously [6]; we assumed the ground vibrational state for the perturber during the collisions and we used the rotational constants B_0 and D_0 of N_2 given in [29]. The electric mutipole moments of CH_3D and N_2 are given in Table 5. The spherical average $u_{000}(r)$ of V_{aa} [30], involved in the trajectory model may be well fitted by a LJ (m–n) potential with $m \approx 6$ and $n \approx 14$. The atom–atom LJ parameters, the intramolecular distances of CH_3D and N_2 the LJ parameters ε, σ, m, and n fitting $u_{000}(r)$ are given in Table 6. By assuming the isotropic part of the potential is described by a 6–14 LJ model such as

$$V_{\mathrm{iso}} = -\frac{C_6}{r^6} + \frac{C_{14}}{r^{14}} \quad \text{with} \quad C_6 = 4\varepsilon\sigma^6 \quad \text{and} \quad C_{14} = 4\varepsilon\sigma^{14}. \tag{8}$$

The vibrational dephasing contribution is obtained from the relative differences $\Delta C_6/C_6$ and $\Delta C_{14}/C_{14}$ between the vibrational matrix elements of this potential as

$$S_1^{\mathrm{iso}} = \frac{3}{2} \frac{\Delta C_6}{C_6} \frac{\pi\varepsilon\sigma}{\hbar v_c'} \left[-\left(\frac{\sigma}{r_c}\right)^5 + \frac{77}{128} \left(\frac{\sigma}{r_c}\right)^{13} y \right], \tag{9}$$

with $\Delta C_6 = (C_6)_{v_f} - (C_6)_{v_i}$ and $y = (\Delta C_{14}/C_{14})/(\Delta C_6/C_6)$. These quantities are not known, so they have been estimat-

Table 5
Molecular parameters for CH_3D and N_2 used in the calculations

Molecule	Q (D Å)	Ω (D Å^2)	Φ (D Å^3)
CH_3D	0	3.10[b]	6.55[b]
N_2	1.40[a]	0	3.4[c]

[a] Ref. [31].
[b] Ref. [32].
[c] Ref. [33].

Table 6
Atom–atom LJ parameters, intramolecular distances r_{1i} of $_3$HCD, r_{2j} of N_2 and LJ (m–n) parameters ε, σ fitting $u_{000}(r)$ for $_3$HCD–N_2 interactions

$\varepsilon_{ii}, \varepsilon_{jj}$ (K)	σ_{ii}, σ_{jj} (Å)	r_{1i}, r_{2j} (Å)	ε (K)	σ (Å)	m	n
$\varepsilon_{C-C} = 61.365$	$\sigma_{C-C} = 3.141$	$\lvert r_{1C}\rvert = 0.0638$				
$\varepsilon_{^3H-^3H} = 14.706$	$\sigma_{^3H-^3H} = 3.845$	$\lvert r_{^3H}\rvert = 0.4313$				
			100.446	3.6969	6.1	13.9
$\varepsilon_{D-D} = 13.232$	$\sigma_{D-D} = 2.662$	$\lvert r_{1D}\rvert = 1.0279$				
$\varepsilon_{N-N} = 37.1625$	$\sigma_{N-N} = 3.290$	$\lvert r_{2N}\rvert = 0.550$				

ed from the experimental data of the self-induced line shifts in the ^QQ-branch of CH_3D as $\Delta C_6/C_6 = 0.008$ and $y = 1$.

The contributions to S_2 include, through the Clebsch–Gordan coefficients, the quantum number K_i and K_f with $K_f = K_i$ for the parallel ν_2 band of CH_3D. For the transitions induced by collisions in the initial and final states, we have only considered $\Delta K = 0$ for the absorber and the usual selection rules for the absorber and perturber molecules, $\Delta J = 0, \pm 1$ for a dipolar transition ($l_1, l_2 = 1$) up to $\Delta J = 0$, ± 1, ± 2, ± 3, ± 4 for a hexadecapolar transition ($l_1, l_2 = 4$).

4.2. Broadening coefficients and comparison with experimental data

The N_2-broadening coefficients were computed for lines at $T = 296$ K in the ^QP-, ^QQ-, and ^QR-branches of the ν_2 band, by including the contributions of N_2 molecules with J_2 values in the fundamental state up to 44 that are weighted by the Boltzmann and nuclear spin factors. The theoretical results are presented in Table 2, and the measured and theoretical results are plotted together in Figs. 5 and 6. Note that in Table 2, we list only the theoretical broadenings that correspond to measured coefficients, whereas in the figures we plot all our calculated coefficients.

The transitions with $K = 3n (n = 1, 2, \ldots)$ are composed of doublets of A_1 and A_2 symmetry, with the selection rule $A_1 \leftrightarrow A_2$, leading to middle terms of the differential cross-section $S_2^{\text{middle}} = 0$ instead of being negative for $l_1 = 1$ or 3 [6]. The influence of this vanishing term strongly increases with increasing n. If the theoretical values for $K = 3$ remain reasonable, the results for $K = 6$ and 9 accounting for the doublet splitting are strongly overestimated. Therefore, we prefer not considering this calculation of broadening coefficients for the doublet components.

The calculated results in the P- and R-branches are practically identical; the negligible differences arise only from the weak contribution of $\mathrm{Im}S_2^{\text{aniso}}(b)$ in Eq. (4). They are presented in Table 2.

In Fig. 5, we have plotted both the measured and theoretical results $\gamma(N_2)$ as a function of $|m|$ for selected transitions in the ^QP-, ^QQ-, and ^QR-branches. Also plotted is a typical error bar. The typical error bar was calculated as the average of all measurement errors for N_2-broadening coefficients from Table 2. For low K ($K \leqslant 3$) with $|m| \leqslant 3$ the theoretical results of the broadening coefficients are in overall good agreement (3.0%) with the experimental data. However, the agreement worsens (5.7 %) for transitions with low K ($K \leqslant 3$) with $|m| \geqslant 12$. The theoretical results of the broadening coefficients are also in overall good agreement (5.3%) with the experimental data for transitions with $K \geqslant 4$. For transitions with $|m| = K + 1$ approaching the theoretical broadening coefficients are generally significantly underestimated (5.9%).

The measured and theoretical N_2-broadening coefficients, $\gamma(N_2)$, as a function of K for constant $|m|$ are plotted in Fig. 6. The typical error bar displayed in Fig. 6 is the same as in Fig. 5. The overall agreement between the measured and calculated broadening coefficients is good. However, as K approaches $|m|$, the agreement worsens and the theoretical results are probably underestimated.

4.3. Lineshift coefficients and comparison with experimental data

The N_2-lineshift coefficients have been calculated at 296 K for lines in the ^QP-, ^QQ-, and ^QR-branches of the ν_2 band. Let us recall that the calculated results have been obtained using the parameter values ($\Delta C_6/C_6 = 0.008$ and $y = 1$) derived from self-induced lineshifts of CH_3D [6]. The theoretical results are presented in Table 2, and the measured and theoretical results are plotted together in Figs. 7 and 8. Note that in Table 2, we list only the theoretical shift coefficients that correspond to measured coefficients, whereas in the figures we plot all our calculated coefficients. Given the scatter of the experimental pressure-induced shifts, δ, the comparison with calculated values is rather difficult. A reasonable agreement is however obtained, although the theoretical results are sometimes larger that the experimental data, as shown in Figs. 7 and 8.

The results in the ^QR-branch are always smaller in absolute value than those in the ^QP-branch, due to the (roughly) antisymmetric component in m of the pressure shift, derived from the pure rotational contribution $\mathrm{Im}(S_2^{\text{aniso}})$ in Eq. (5). This is not in contradiction with the experimental results which are generally smaller in absolute value in the ^QR-branch than in the ^QP-branch. Here, the pure rotational contribution corresponding to the half-difference between the results in the P- the R-branches (asymmetric component of the line shifts [34]) is much smaller in magnitude, especially for medium or high J transitions, than the vibrational contribution to the shifts given by the results in the Q-branch.

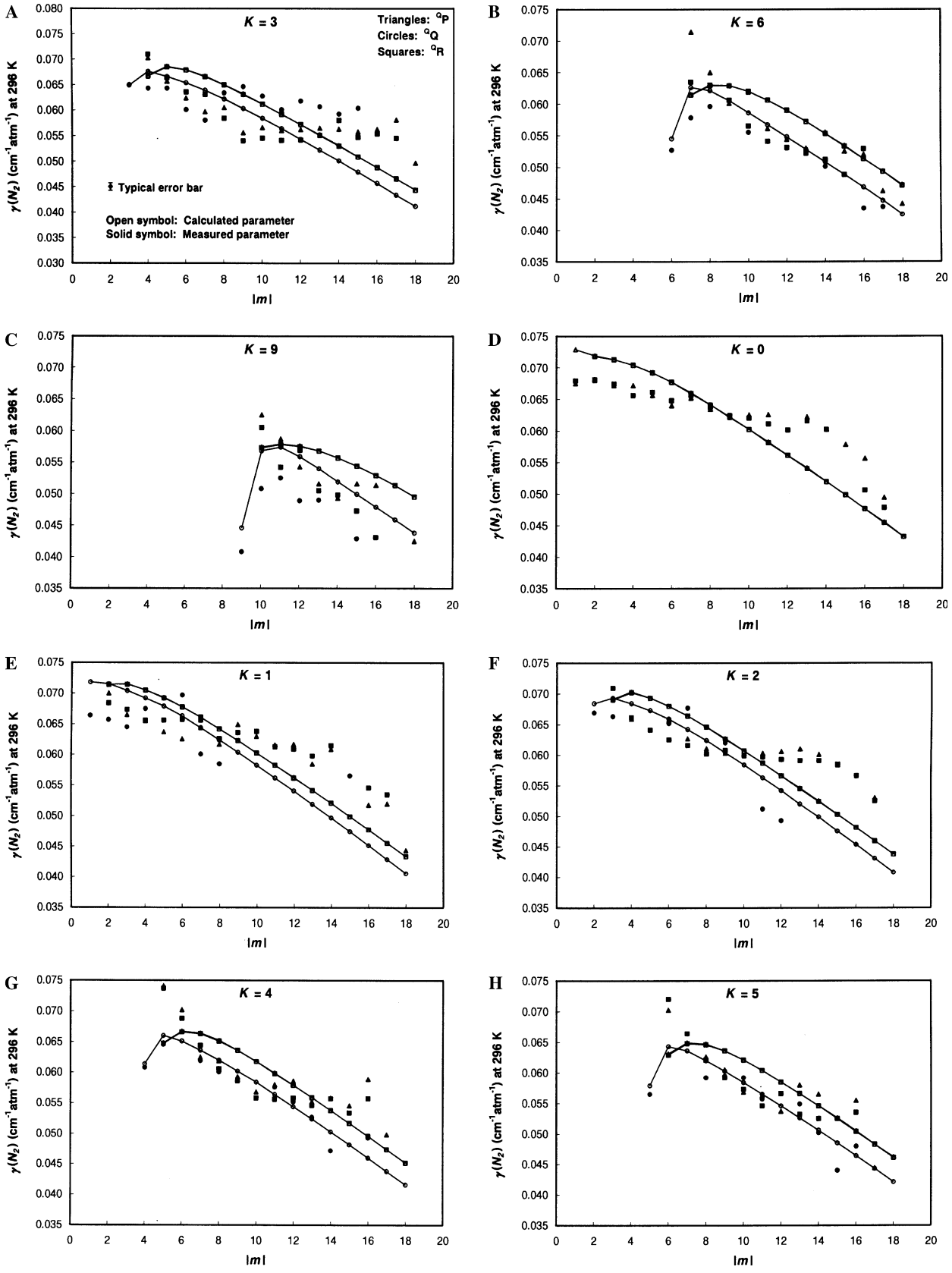

Fig. 5. Variation of measured, empirically derived, and theoretically calculated N_2-broadening coefficients with $|m|$ for (A) $K=3$; (B) $K=6$; (C) $K=9$; (D) $K=0$; (E) $K=1$; (F) $K=2$; (G) $K=4$; and (H) $K=5$. For a given $|m|$, the theoretical broadening coefficients for the ${}^{Q}P$ and ${}^{Q}R$ lines are very nearly the same.

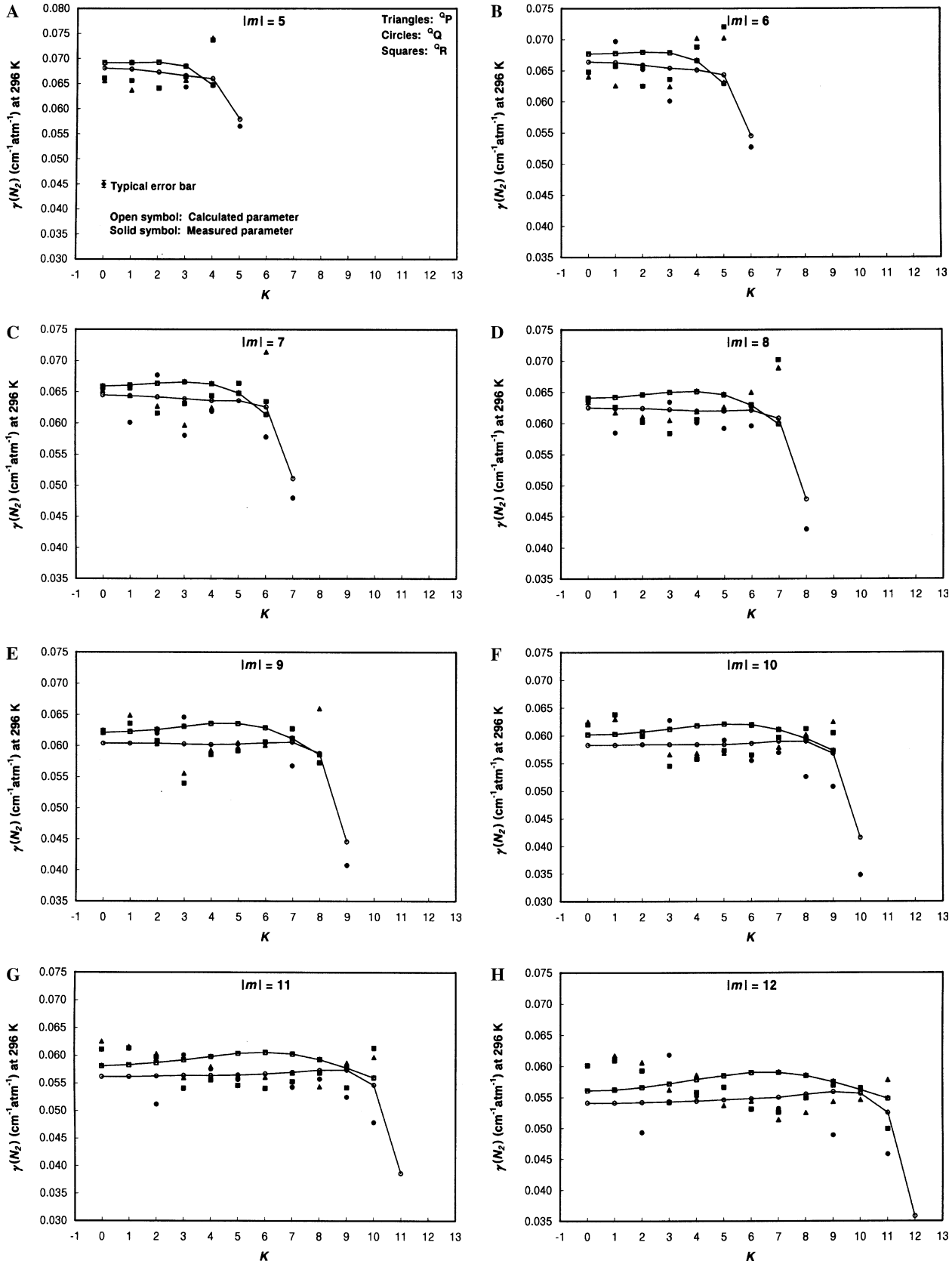

Fig. 6. Variation of measured, empirically derived, and theoretically calculated $\gamma(N_2)$ versus K in select $|m|$ series ($|m| = 5$–12, in panels A–H, respectively) in the ^{Q}P-, ^{Q}Q-, and ^{Q}R-branches.

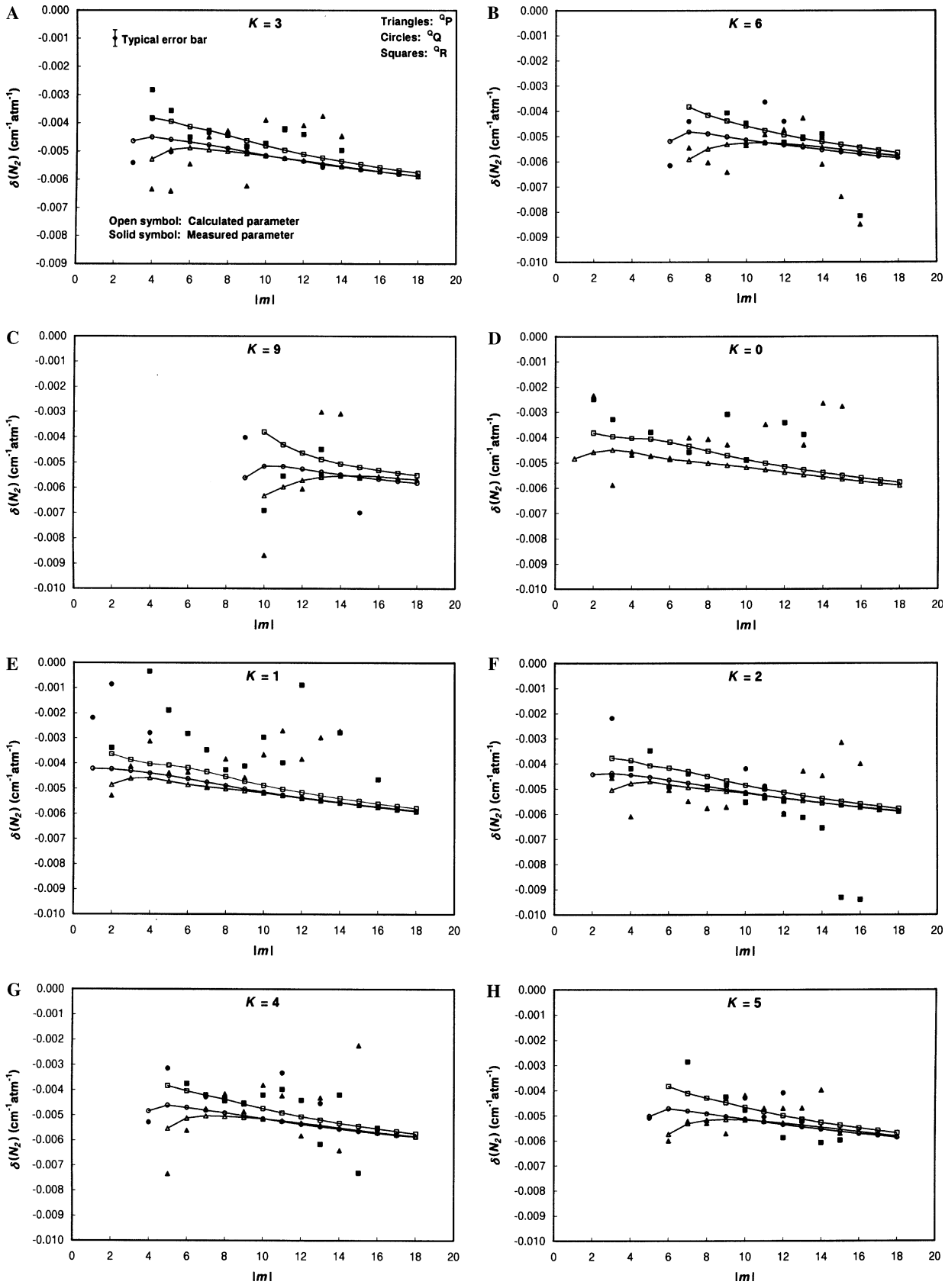

Fig. 7. Measured and theoretical N_2-induced pressure-shift coefficients, $\delta(N_2)$ as a function of $|m|$ for selected K series transitions: (A) $K = 3$, (B) $K = 6$, (C) $K = 9$, (D) $K = 0$, (E) $K = 1$, (F) $K = 2$, (G) $K = 4$, and (H) $K = 5$.

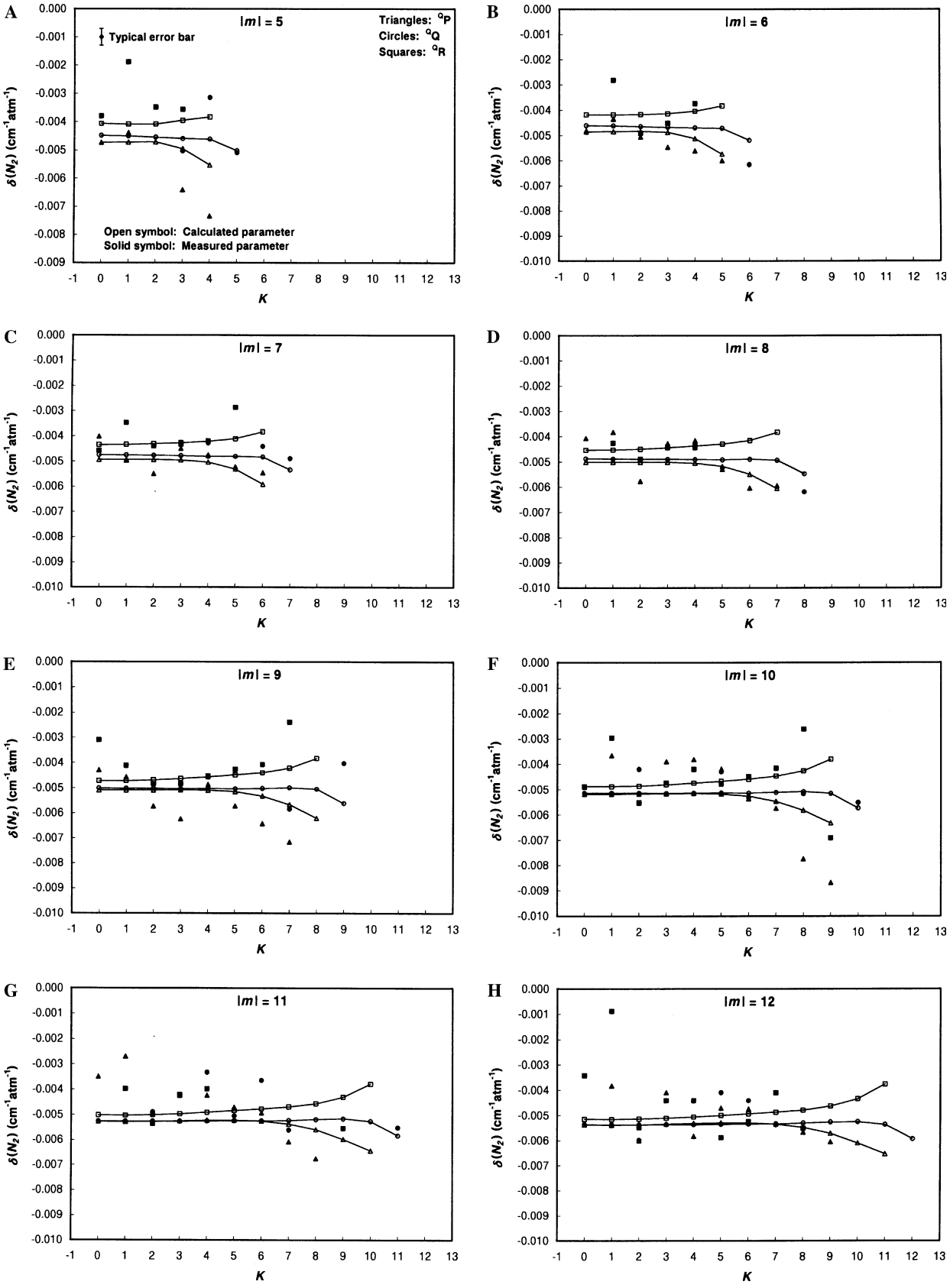

Fig. 8. Theoretically calculated and measured N_2-shift coefficients, $\delta(N_2)$, as a function of K for (A) $|m| = 5$, (B) $|m| = 6$, (C) $|m| = 7$, (D) $|m| = 8$, (E) $|m| = 9$, (F) $|m| = 10$, (G) $|m| = 11$, and (H) $|m| = 12$.

Several interesting trends are revealed in the measured N_2-shift coefficients when they are plotted in Fig. 7 as a function $|m|$ for various K series. The ^QR-branch coefficients for low K show an interesting pattern where they tend from small negative values at low $|m|$ towards more negative values. The pattern exhibits a minimum in the vicinity of $|m| = 8$–10. At higher $|m|$ values the shift coefficients begin to increase towards less negative values. The result is a concave up shape to the graphs. At higher K values the concave up shape is less pronounced and it is followed by a sharply decreasing trend in the shift coefficients at high $|m|$. The ^QP-branch shift coefficients follow a different trend with $|m|$ that appears to be oscillatory. It is difficult to recognize a trend in the ^QQ-branch transitions due to the relatively small number of data points. The theoretical results show reasonable agreement with the experimental shift coefficients but they do not seem to reproduce the observed trends in the experimental data.

The N_2-shift coefficients also show interesting trends with K, as revealed in Fig. 8. The ^QR-branch shift coefficients for $|m| = 7$–10 display fairly prominent concave up shapes with minimum around $K = 3$. The theoretical calculations reproduce the tendency of the ^QR-branch shift coefficients to increase with decreasing K fairly well. The general trend in the ^QP-branch shift coefficients is to remain nearly constant for early K values, then to fall off more and more rapidly to more negative values as K approaches $|m|$. This trend is well defined in the theoretical results for the ^QP-branch as well.

5. Conclusion

This work presents experimental measurements and theoretical calculations of N_2-induced pressure-broadening and -shift coefficients in the ν_2 band of the CH_3D molecule. Analyzing 11 FTIR spectra, we have determined accurate values for zero-pressure line center positions, N_2-broadening coefficients and N_2 pressure-induced shift coefficients for 368 transitions. The data presented in this work have revealed several interesting patterns in the measured pressure-broadening and pressure-induced shift coefficients. The empirical expressions derived to compute the N_2-broadening coefficients as a function of $|m|(|m|+1)$ and K^2 reproduce our measurements within 4.7%, will be useful for remote sensing applications.

The theoretical results are very satisfactory by considering the main approximation used in the calculations, i.e., the CH_3D molecule is treated as a linear molecule for its interactions with N_2. Moreover the values of the potential parameters used in the calculations of broadening coefficients were all taken from sources available in the literature and were not adjusted to fit any data. The agreement of calculated and experimental results is quite good (6.4% for transitions with J'' below 14), except for $K = J$ or $K = J - 1$ where the results seems to be underestimated (7.4%). We have shown that the line shifts mainly originate from vibrational dephasing effects. Unfortunately, the data of pressure shifts are generally scattered and, therefore, do not allow us to test accurately our theoretical model.

Acknowledgments

We are very grateful to Dr. Linda R. Brown from the Jet Propulsion laboratory (JPL), California Institute of Technology for allowing us to use her self-broadened CH_3D spectra. Our gratitude also goes to Dr. D. Chris Benner from the College of William and Mary for offering his multispectrum fit program. We thank Dr. Malathy Devi from the College of William and Mary for her advice in handling the spectra and the analysis with the multispectrum fit program. A. Predoi-Cross acknowledges the support she received from the National Sciences and Engineering Research Council of Canada and the Summer Temporary Employment Program of the Government of Canada. The research at the NASA Langley Research Center was performed under contracts with the National Aeronautics and Space Administration. We also thank NASA's Upper Atmosphere Research Program for their support of the McMath-Pierce FTS laboratory facility.

References

[1] T. Fouchet, E. Lellouch, Icarus 144 (2000) 114–123.
[2] M.D. Smith, B.J. Conrath, D. Gautier, Icarus 124 (1996) 598–607.
[3] O. Mousis, D. Gautier, A. Coustenis, Icarus 159 (2002) 156–165.
[4] C. Boussin, B.L. Lutz, A. Hamdouni, C. de Bergh, J. Quant. Spectrosc. Radiat. Transfer 63 (1999) 49–84.
[5] C. Boussin, B.L. Lutz, C. de Bergh, A. Hamdouni, J. Quant. Spectrosc. Radiat. Transfer 60 (1998) 501–514.
[6] A. Predoi-Cross, K. Hambrook, M. Brawley-Tremblay, J.-P. Bouanich, M.V. Devi, D.C. Benner, L.R. Brown, J. Mol. Spectrosc. 234 (2005) 62–83.
[7] V.M. Devi, D.C. Benner, M.A.H. Smith, C.P. Rinsland, L.R. Brown, J. Quant. Spectrosc. Radiat. Transfer 73 (2002) 603–640.
[8] V.M. Malathy Devi, D.C. Benner, M.A.H. Smith, C.P. Rinsland, L.R. Brown, J. Quant. Spectrosc. Radiat. Transfer 74 (2002) 1–41.
[9] V.M. Devi, D.C. Benner, M.A.H. Smith, C.P. Rinsland, L.R. Brown, R.L. Sams, S.W. Sharpe, J. Quant. Spectrosc. Radiat. Transfer 72 (2002) 139–191.
[10] P. Varansai, S. Chudamani, Appl. Opt. 28 (1989) 2119–2122.
[11] N. Lacome, F. Cappellani, G. Restelli, Appl. Opt. 26 (1987) 766–768.
[12] V.M. Devi, D.C. Benner, M.A.H. Smith, C.P. Rinsland, K.B. Thakur, J. Mol. Spectrosc. 122 (1987) 182–189.
[13] V.M. Devi, C.P. Rinsland, D.C. Benner, M.A.H. Smith, K.B. Thakur, Appl. Opt. 25 (1986) 1848–1853.
[14] G. Blanquet, J. Walrand, J.-P. Bouanich, J. Mol. Spectrosc. 171 (1995) 525–532.
[15] J. Walrand, G. Blanquet, J.-P. Bouanich, Spectrochim. Acta A 52 (1996) 1037–1040.
[16] P. Varanasi, L.P. Giver, F.P.J. Valero, J. Quant. Spectrosc. Radiat. Transfer 30 (1983) 511–516.
[17] S. Chudamani, P. Varanasi, J. Quant. Spectrosc. Radiat. Transfer 38 (1987) 179–181.
[18] G.D.T. Tejwani, K. Fox, J. Chem. Phys. 61 (3) (1974) 759–762.
[19] C.J. Tsao, B. Curnutte, J. Quant. Spectrosc. Radiat. Transfer 2 (1962) 41–91.
[20] D. Robert, J. Bonamy, J. Phys. (Paris) 40 (1979) 923–943.
[21] R.P. Leavitt, J. Chem. Phys. 73 (1980) 5432–5450.

[22] C. Lerot, J. Walrand, G. Blanquet, J.-P. Bouanich, M. Lepère, J. Mol. Spectrosc. 217 (2003) 79–86.
[23] D.C Benner, C.P. Rinsland, V.M. Devi, M.A.H. Smith, D. Atkins, J. Quant. Spectrosc. Radiat. Transfer 53 (1995) 705–721.
[24] R.A. Toth, J. Opt. Soc. Am. B. 8 (1991) 2236–2255.
[25] R.P. Leavitt, D. Korff, J. Chem. Phys. 74 (1980) 2180–2188.
[26] L. Ozier, W. Ho, G. Birnbaum, J. Chem. Phys. 51 (1969) 4873–4880.
[27] J. Bonamy, L. Bonamy, D. Robert, J. Chem. Phys. 67 (1977) 4441–4453.
[28] J.-P. Bouanich, J. Quant. Spectrosc. Radiat. Transfer 47 (1992) 243–250.
[29] D. Reuter, D.E. Jennings, J.W. Brault, J. Mol. Spectrosc. 115 (1986) 294–304.
[30] J.-P. Bouanich, D. Lambot, G. Blanquet, J. Walrand, J. Mol. Spectrosc. 140 (1990) 195–213.
[31] W.H. Flygare, R.C. Benson, Mol. Phys. 20 (1971) 225–250.
[32] K. Jacquiez, G. Blanquet, J. Walrand, J.-P. Bouanich, J. Mol. Spectrosc. 171 (1996) 386–389.
[33] N.W.B. Stone, L.A.A. Read, A. Anderson, I.R. Dagg, W. Smith, Can. J. Phys. 62 (1984) 338–347.
[34] A. Predoi-Cross, J.-P. Bouanich, D.C. Benner, A.D. May, J.R. Drummond, J. Chem. Phys. 113 (2000) 158–168.